TU Delft

Delft University of Technology

Change lost

Corrosion of Roman copper alloy coins in changing and variable burial environments

Huisman, Luc Hans; Ackermann, Regula ; Claes, Liesbeth ; van Eijck, L.; de Groot, Tessa ; Joosten, Ineke; Kemmers, Fleur ; Kerkhoven, Nils ; Ngan-Tillard, D.J.M.; More Authors

DOI
10.1016/j.jasrep.2022.103799

Publication date
2023

Document Version
Final published version

Published in
Journal of Archaeological Science: Reports

Citation (APA)
Huisman, L. H., Ackermann, R., Claes, L., van Eijck, L., de Groot, T., Joosten, I., Kemmers, F., Kerkhoven, N., Ngan-Tillard, D. J. M., & More Authors (2023). Change lost: Corrosion of Roman copper alloy coins in changing and variable burial environments. *Journal of Archaeological Science: Reports*, *47*, Article 103799. https://doi.org/10.1016/j.jasrep.2022.103799

Important note
To cite this publication, please use the final published version (if applicable).
Please check the document version above.

Copyright
Other than for strictly personal use, it is not permitted to download, forward or distribute the text or part of it, without the consent of the author(s) and/or copyright holder(s), unless the work is under an open content license such as Creative Commons.

Takedown policy
Please contact us and provide details if you believe this document breaches copyrights.
We will remove access to the work immediately and investigate your claim.

This work is downloaded from Delft University of Technology.
For technical reasons the number of authors shown on this cover page is limited to a maximum of 10.

Journal of Archaeological Science: Reports 47 (2023) 103799

Contents lists available at ScienceDirect

Journal of Archaeological Science: Reports

journal homepage: www.elsevier.com/locate/jasrep

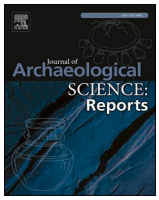

Change lost: Corrosion of Roman copper alloy coins in changing and variable burial environments

Hans Huisman [a,b,*], Regula Ackermann [c], Liesbeth Claes [d], Lambert van Eijck [e], Tessa de Groot [a], Ineke Joosten [a], Fleur Kemmers [f], Nils Kerkhoven [g], Jan-Willem de Kort [a], Sarah Lo Russo [h,i], Dominique Ngan-Tillard [e], Bertil van Os [a], Markus Peter [j], Christine Pümpin [h], Jeroen Vaars [k], Zhou Zhou [e,l]

[a] *Cultural Heritage Agency of the Netherlands, the Netherlands*
[b] *University of Groningen, the Netherlands*
[c] *Kantonsarchäologie St.Gallen, Switzerland*
[d] *Leiden University, the Netherlands*
[e] *Technische Universiteit Delft, Faculty of Applied Sciences, Delft, the Netherlands*
[f] *Goethe University, Frankfurt am Main, Germany*
[g] *Erfgoed Utrecht, the Netherlands*
[h] *Integrative Prehistory and Archaeological Science (IPAS), University of Basel, Switzerland*
[i] *Maritime Cultures Research Institute, Vrije Universiteit Brussel, Belgium*
[j] *Augusta Raurica, Switzerland*
[k] *Archeologenbureau Argo, the Netherlands*
[l] *Reactor Institute Delft, the Netherlands*

A R T I C L E I N F O

Keywords:
Coin
Corrosion
Gley
Sulphides
Tomography

A B S T R A C T

We studied the corrosion of Roman copper alloy coins that experienced alternations or progressive changes in their burial environment. We used coins that were still embedded in soil or in a concretion selected from three professional excataved sites - Berlicum and Krommenie in the Netherlands and Kempraten in Switserland. mCT scanning and neutron scanning were used to record the 3-D properties of these coins prior to (destructive) analyses. It proved possible to tentatively identify the coins. Microscope observations and SEM-EDX analyses revealed complex corrosion processes, related to changing burial environments. In soil horizon with fluctuating groundwater levels in a region with upwelling reducing, iron-rich groundwater, the copper in a gunmetal coin is essentially replaced by iron oxides while tin remains and forms tin-oxide bands. Fluctuating redox conditions in marine-influenced environments was shown to transform a copper-alloy coin into strongly laminated copper sulphides with embedded gypsum crystals, with an outer surface of copper and copper-iron sulphides. Burial of bronze in a charcoal rich layer probably caused temporary highly alkaline soil conditions. This caused most of the copper to leach from this coin, leaving behind a laminated tin-dominated mass, with only a limited amount of (malachite) corrosion products remaining in the surrounding groundmass. In all three cases, corrosion processes tend to be anisotropic, probably because of cold-hammering of the coins during their manufacture. Such corrosion processes on massive copper alloy coins may produce features that may lead to their incorrect classification as *subferrati,* i.e. copper alloy coins with an iron core. Our results may help in future to distinguish strongly corroded massive coins from *subferrati*.

* Corresponding author.
E-mail address: hans.huisman@rug.nl (H. Huisman).

https://doi.org/10.1016/j.jasrep.2022.103799
Received 2 May 2022; Received in revised form 21 November 2022; Accepted 14 December 2022
Available online 5 January 2023
2352-409X/© 2022 The Author(s). Published by Elsevier Ltd. This is an open access article under the CC BY license (http://creativecommons.org/licenses/by/4.0/).

1. Introduction

1.1. Study rationale

Since the start of copper working and alloying, copper alloys form a substantial and important component of the archaeological record. Typology, spatial distribution, compositional variation, isotope ratios and use wear-related features bear witness to e.g. cultural and technical developments, spread of raw materials and technology and specific human activities like burial rites, depositions and warfare. An additional dimension of copper alloy objects to the archaeological record came with the first use of copper alloys for coins ca. the 5th century BCE (e.g. Brousseau 2010): Since then, copper alloy coins from the archaeological record provide direct information on socio-economic and geopolitical developments as well as means to give a rather good *terminus post quem* date for archaeological features.

One of the reasons why copper alloy objects form a major component of the archaeological record is that in many burial environments they are often fairly well preserved. Although copper does corrode – it is oxidized by oxygen and by hydrogen sulphide – it can form a stable corrosion crust or a passivation layer on the outside surface of the objects, which prevents it against further corrosion in most environments. As a result, copper alloy objects from thousands of years ago can still be studied and displayed, despite a crust or patina caused by corrosion. This does not mean that all is well. E.g. copper alloy coins in practice appear to be corroded very badly. Their small size and the importance of surface detail for their identification may play a role, but it may also indicate that more copper alloy objects have been lost from the archaeological record than we realize. E.g. green stains in the soil have been observed in several Roman sites in the coastal area of the Netherlands, indicating that Roman copper alloy objects have completely disintegrated (*pers. comm.* Van der Feijst, Archeologisch Dienstencentrum Amersfoort), leaving nothing but corrosion products. Similar observations were e.g. done at the excavation of a Mithraeum in Kempraten (Ackermann et al. 2020). There, also, coins were sometimes corroded to such a degree that they were undetected by metal detectors. Some of these were lost during the restauration process because after the removal of corrosion layers there was no uncorroded core left. The sensitivity of archaeological copper alloys to corrosion is a reason that the corrosion processes and burial environments have received much attention in past research (Robbiola et al. 1998, Scott 2002, Selwyn 2004, Ingo et al. 2006, Huisman & Joosten, 2009, Nienhuis et al. 2016, Nienhuis 2017, Oudbashi 2018, Oudbashi et al. 2019, Rémazeilles et al. 2020).

Coins that consist of an iron core, with copper coating (so-called *subferrati;* Doyen et al. 2017 for a recent overview), are potentially more affected, as iron is much more prone to oxidation than copper. Under corrosion, these coins tend to deform and burst open from the inside due to the preferential corrosion of the iron in the core. Numismatic specialists sometimes use magnets to test whether strongly corroded coins are indeed *subferrati,* but this can only work if metallic remnants of the iron core are still present.

Many of the corrosion studies seem to be based on finds from two types of burial environments, i.e. well-drained terrestrial soils and seafloor environments, or on heritage objects that were in the open air. Even when other environments are mentioned or described, the examples given often give the impression that the effects of corrosion on the objects have been minor, and that proper conservation is enough to prevent loss of archaeological information or heritage values (c.f. Scott 2002). Material from other environments, like acid-sulphate soils, gley zones and ash- and charcoal- influenced anthropogenic deposits seems to have received much less attention. As a result, an implicit idea may form that copper alloy objects preserve well in all burial environments. This idea would be incorrect, however, and survival of copper alloy objects in the archaeological record is probably much more dependent on various post-depositional conditions and processes in the burial environment than may be apparent from the literature.

Moreover, most corrosion studies were done on objects that had already been excavated or recovered, cleaned and often conserved and restored (Scott 2002, Selwyn 2004). Recent studies in iron corrosion (Matthiesen et al. 2007, Neff et al. 2007) have shown that the corrosion processes of buried objects encompasses not only the object but also its surrounding soil as well. Understanding the corrosion system therefore needs to take into account both the object, the surrounding soil and the transition between the two. This aspect seems to be missing in most of the literature on copper alloy corrosion, even though they may be of prime importance for understanding corrosion processes in specific environments and their impact on the survival and preservation of copper alloy objects, and their identification.

In the present work, we report on a study of copper alloy objects (coins) from three environments that have received little or no attention in corrosion literature, and for which the corrosion systems are therefore understated in archaeological, archaeometric and conservation literature. In order to understand the corrosion system and its impact on the preservation of the objects, we studied the objects as much as possible within their original soil environment, i.e. without removing corrosion scales or adhering soil material. The results are relevant for understanding the preservation of copper alloy objects in specific environments. Moreover, it showed how specific corrosion processes can result in misclassification of coin types (i.c. *subferrati*).

1.2. Knowledge base copper alloy corrosion

Copper is unstable in oxidic environments, and will start to corrode. In some burial environments, the initially formed corrosion products will prohibit further corrosion ("passive" corrosion), in other environments corrosion will proceed despite the corrosion products ("active" corrosion). The Pourbaix diagrams in Fig. 1 A-C indicate under different acidity and redox conditions metallic copper is stable, and which species form when corrosion occurs. Fig. 1D demonstrates the much greater stability of silver. Fig. 2 shows what kind of corrosion layers and patinas can form under different burial conditions.

When occurring in oxidic moist or wet soil environments, corrosion of copper usually results in an outer layer of copper carbonate (malachite or azurite) on top of copper oxides (cuprite; Fig. 2A; see also Robbiola et al. 1998, Oudbashi 2018). Despite the relative stability of this outer layer, some leaching and reprecipitation of copper into the surrounding soil environment seems to occur; that is e.g. the reason that organic remains can remain preserved in the immediate vicinity of copper alloy objects (cf. Huisman et al., 2009; Huisman and Joosten, 2009). In cases where cavities are present in or surrounding a copper alloy object, malachite can form typical curly minerals that resembles organic materials (Scott 2002, Nienhuis et al. 2016). In marine, arid or other saline environments, chloride (Cl^-) ions may play a role as well. Although they play no direct role in the oxidation processes *sensu strictu*, they may speed up the process, and they may form minerals with the corrosion products. Typically, copper chlorides may form on the contact between the metal and the oxides (Fig. 2B; see also Oudbashi et al. 2019).

In marine and estuarine environments, metal attack is triggered by sulphate reducing bacteria (SRB) (Johnson & Hallberg, 2005, King et al. 2011, Little et al. 1991, Little et al. 2000a,b, Little & Wagner 2018, McNeil et al. 1991, McNeil & Little 1999, Wiener et al. 2006). Generally this attack starts as biofilms attached to the oxidized metal surface where SRB's partly remove the passive oxide layer. If reduced iron is present in such environments, its oxidation towards iron hydroxides will be promoted by dissolved copper, causing low-pH micro-environments. In these environments, a corrosion layer is formed that consists of copper sulphides like chalcocite (Cu_2S) and/or covelite (CuS). Sometimes a layer of chalcopyrite ($CuFeS_2$) forms, if enough dissolved iron is available in the burial environment (Fig. 2 C,D). In reducing non-sulphidic environments, no copper alloy corrosion seems to occur. Copper corrosion is dependent on the availability of reactants (oxidants and

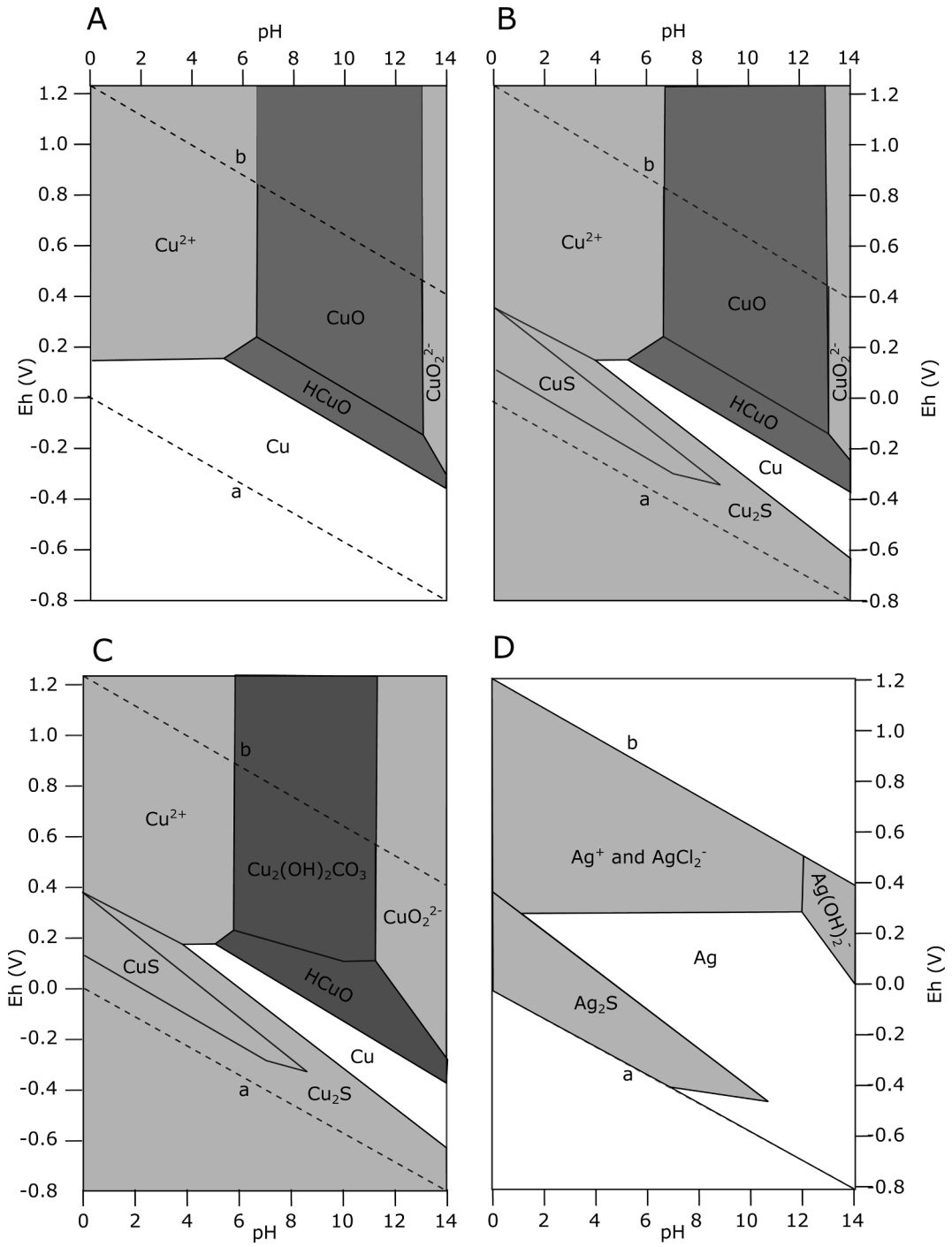

Fig. 1. Pourbaix diagrams and stability fields of copper (Cu) and silver (Ag) (25 °C, 1 atm.). Redrawn after Brookins (1988) and Selwyn (2004). A: Pourbaix diagram and stability fields of copper ([Cu] = 10^{-6} [S] = 0). This diagram indicates under which redox and acidity conditions the different phases of copper, oxygen and hydrogen are stable in the soil. Regions are labelled with the thermodynamically stable species (phase) in that region. The stability region of the water is shown by the broken lines (a and b). Shading indicates fields where copper is immune (the metal is stable; white), passive (the corrosion products are insoluble and stable; dark grey) and active (corrosion products are dissolved ions; light grey) after Selwyn (2004). B: Pourbaix diagram of copper in environments with sulphate and sulphide species ([Cu] = 10^{-6}, [S] = 10^{-3}). Note that a large part of the area that was immune in A is now taken over with Cu-S corrosion products. C: Idem, with available carbonates ([C] = 10^{-1}). In the passive field, the oxides are partially replaced by Malachite (carbonate). D: Pourbaix diagram for silver ([Ag] = 10^{-8}; [S = 10^{-3}]). Native sulphur is stable in most of the field, but at low pH, corrosion can occur: Transitions to silver sulphides low Eh, and at higher Eh dissolution as Ag^{+-} or (in the presence of chlorides) $AgCl_2^-$. At very high pH and Eh, metallic silver can dissolve to form $Ag(OH)_2^{2-}$ species.

protons). In sediments or soils with low porosity, e.g. silts (Martinón-Torrez et al. 2019) or massive clays, water movement and availability of reactants is restricted. Under such conditions, oxidants such as sulphate, locally available iron or oxygen will be depleted rapidly, bringing corrosion processes to a halt.

The corrosion effects are more complex when alloying metals like tin (Sn), zinc (Zn) and lead (Pb) are taken into account: Zn in copper alloys like brass and gunmetal is preferably corroded and leached. Tin is resistant to leaching – even when oxidized – and can therefore be relatively enriched at the surfaces of corroded bronzes. High-tin bronzes are

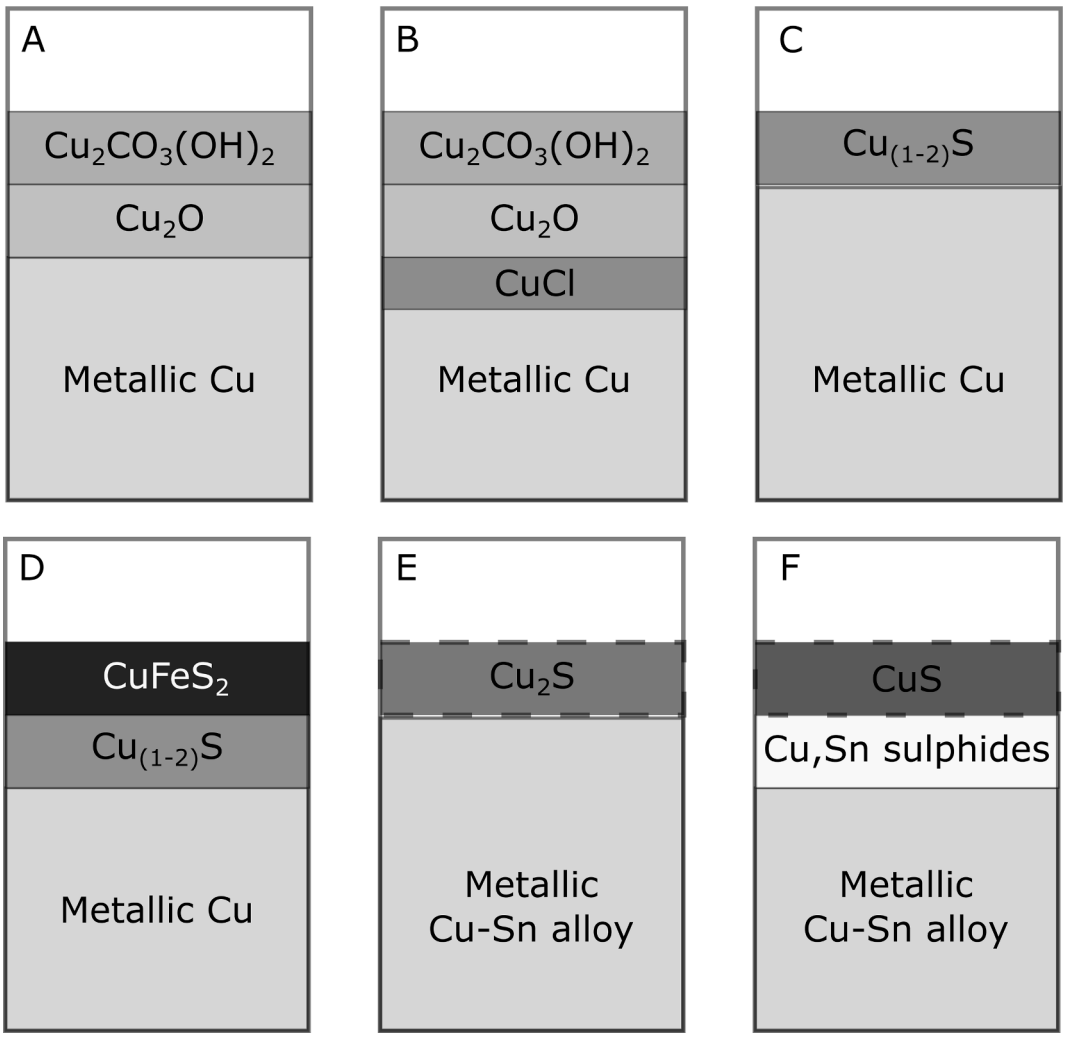

Fig. 2. Schematic overview of copper alloy corrosion layers that may form in different environments. Based on Robbiola et al. (1998), McNeil & Little (1999), Scott (2002), Selwyn (2004), Ingo et al. (2006), Huisman and Joosten (2009) and Rémazeilles et al. (2020). A: Corrosion of copper alloys in oxidic burial environment typically result in a corrosion layer of malachite on top of cuprite. B: In oxidic saline or marine environments, a thin layer of copper chlorides can form between the metallic copper alloy and the cuprite layer. C: In sulphidic environments, a porous layer of copper sulphide forms. D: If Fe^{2+} is available in a sulfidic environment, a layer of chalcopyrite ($CuFeS_2$) can develop on top of the supper sulphide layer. E, F represent a complex corrosion sequence (described by Rémazeilles et al. 2020) whereby oxic corrosion is followed by burial in an anaerobic environment where the oxic corrosion products are transformed into Cu_2S (in E), after which further corrosion and transformation processes result in a CuS layer overlying a layer with Cu,Sn sulphides. The thick broken lines indicates that iron-rich layers can occur on the surface (type A), or on the transition from copper sulphide to Cu,Sn sulphide layers (type A and B respectively according to Rémazeilles et al. 2020).

known to be corrosion-resistant because a passive tin-rich layer forms at their surface during corrosion. However, Rémazeilles et al. (2020) indicated that complex Cu,Sn sulphides can form below the Cu,S corrosion layer during sulphidic corrosion of bronzes (Fig. 2 E,F). Lead, mostly present as a separate metallic phase in copper alloys, oxidizes readily in all natural environments. Corrosion products like $PbCO_3$, various oxides, PbS and $PbSO_4$ are stable, but in environments that lack sulphidic species, lead can go into solution at pH < 5 (Brookins 1988). In corrosion layers, lead species can accumulate at the boundary between corroded metal and external corrosion layer (Martinón-Torres et al. 2007). These reactions, however, have little or no effect on the overall corrosion and passivation of copper alloy objects, which is dominated by the behaviour of copper.

In contrast to copper, silver tends to be stable in a large part of the Eh-Ph diagram (Fig. 1D). Under strongly reducing conditions, stable silver sulphides (AgS_2) may form. Oxidized species that can dissolve can only form at high Eh; at low and neutral pH Ag^+ or – if chloride is present – $AgCl_2^-$, at high pH $Ag(OH)_2^-$.

1.3. Lacunae

As indicated above, the burial environment determines which copper corrosion products will be formed and their stability. In an open system such as in a porous soil or sediment, reactants (H^+ ions, oxygen, sulphide, dissolved iron) will be transported according to flow rates, diffusion and gradients. In such cases copper corrosion processes will not slow down as reactants are continuously transported away from the object and eventually precipitate according to chemical gradients. Here, and in corrosion literature in general, an implicit assumption is that the burial environment has been stable since the objects were buried. This is a fair assumption under most circumstances, but not in all cases. E.g. fluctuating redox conditions can cause periodic interference of reactive species (e.g. dissolved ferrous iron) with the corrosion and precipitation processes, whereas progressive changes in soil chemistry (e.g. pH change) may cause changes in the stability of metals and corrosion products.

Burial environments that have not received sufficient attention include:

- Burial environments with fluctuating chemical conditions: This is e. g. the case in those soil horizons where variable groundwater levels cause alternations between oxic and reducing conditions. Specific for such conditions is not only the alternation between different redox conditions: In freshwater environments, each reducing phase sees the emergence of $Fe^{2+}_{(aq)}$ from reduction of iron oxides or through groundwater transport whereas these compounds precipitate as Fe (III) oxyhydroxides during oxic phases. This precipitation reaction in addition has an acidifying effect as well. This acidification, the Fe^{2+} ions and the precipitation of Fe(III) compounds all have the potential to interfere with the corrosion process of copper alloy objects by promoting dissolution of specific compounds, redox-reactions and by new-forming of minerals.
- Sulphidic environments with low pH: Under reduced saline or brackish conditions, reduced iron compounds typically form mono- and disulphides such as pyrite or pyrrhotite (FeS_2, FeS) due to a higher availability of sulphur compounds. Oxidation of such compounds during phases of lowering water tables result in acidification and the formation of Fe(III) oxyhydroxides, as well as jarosite (K,Na) $Fe_3(SO_4)_2(OH)_6$) or – if calcium carbonate (shells) is present in the sediment – gypsum ($CaSO_4$). These reactions may as well influence copper corrosion mechanisms. Our knowledge on the corrosion of archaeological copper in sulphidic environments is based on finds from seafloor contexts. In these contexts, the pH (seawater and porewater) is buffered by high alkalinity. However, in sulphidic environments with low alkalinity – like marine-influenced coastal peat deposits – pH values may drop, facilitating the progressive corrosion of copper alloys.
- Fire-affected burial conditions: Many archaeological contexts show evidence for fire, especially in settlements. The impact of fire on corrosion of copper alloy objects is therefore of prime importance. This impact is twofold. Firstly, the metallic surface of copper alloy objects that were heated to temperatures over 300 °C in an oxidizing environment before deposition (e.g. in cremation burials) can be altered into tenorite (CuO), a mineral that is resistant to further corrosion (Ratnawulan et al. 2017, Nienhuis 2017). Secondly, wood fire produces ash that is dominated by Ca- and K-hydroxides. This has a major influence on the pH and dissolved species in the burial environment: If objects become buried in archaeological contexts that are rich in wood-ash, they will at first experience strongly alkaline conditions at the moment of burial. This alkalinity is strong enough to e.g. degrade organic material and to promote the displacement of clays (Huisman et al. 2012, 2017). In open-air sites, these conditions are usually short-lived, though: Rain and percolating soil water will quickly dissolve and leach potassium hydroxide whereas calcium hydroxide is mostly transformed into carbonates, buffering soil pH around 8.0–8.2. In most environments, apart from dry climates and dry cave settings, strong alkaline conditions will therefore quickly disappear and will be replaced by lime-buffered burial conditions. The potential impact of this relatively short-lived burial phase with strong alkaline conditions on the corrosion of copper alloy objects is unknown.

In this publication, we present our research on three cases of copper corrosion in Roman coins in various environments: One from a terrestrial context with variable redox conditions, one from a coastal peat setting and one that has potentially been affected by fire and ash-induced high alkalinity. Two of these cases (Krommenie and Berlicum) can be seen as examples where the corrosion processes may affect the interpretation of the coin type: Here, the coins were macroscopically first tentatively classified as *subferrati*: coins consisting of a copper alloy plate surrounding an iron core. This classification was not tested with a magnet, but based on macroscopic observations only. *Subferrati* are attested in *Gallia Belgica* and the provinces of Germania from AD 20/30 – AD 60/70, and in NW Gaul and Danubia starting AD 160, and disappearing completely shortly after AD 260 (Doyen et al. 2017). A small number are reported from sites in the Netherlands. E.g. Doyen et al. (2017) mention 32 bronze *subferrati* found in the Netherlands up to May 2017, whereas 50 subferrati could be found in the Dutch national coin finds database NUMIS in 2022 (P. Beliën *pers. comm.* 2022).

It is unclear to what extent their classification was tested with a magnet, or only based on macroscopic observations as well; in several cases the classification is based on weight. In this context it is highly relevant to confirm presumed *subferrati* identifications – like the ones from Krommenie and Berlicum - or to determine that they give this impression simply due to their macroscopic appearance after corrosion processes in a specific environment. With these results the other recorded *subferrati* finds from the Netherlands will have to be newly evaluated.

Interestingly, studies on Roman silver coins from Velsen and Uitgeest – both ~ 5 km from Krommenie – have shown considerable corrosion as well: Silver *denarii* from the 1st century CE Velzen I and Velzen II Roman fleet base were found to be corroded completely into silver sulphides (especially Ag_2S). The adultered (4–40 % Cu) silver coins from a second-century Roman hoard found at Uitgeest were found to have transformed into concretions, with on the inside alternating laminae of CuS and Ag_2S. In both cases, macroscopic features led the researchers first to believe these coins were plated, or *subaerate denarii* (Vons 1983, 1987). Here also, the coin surfaces were read by splitting apart the concretion in order to read the impression of the coin on the corrosion crust (Vons 1977).

1.4. Approach

In this study, we use a combination of techniques to characterize the impact of corrosion processes on the coins, and properties of the corrosion layer. As these techniques (optical microscopy, SEM-EDX) are employed on a cross-section of the coins while embedded in corrosion products or resin, they were first scanned in order to try and make identification possible prior to the destructive research activities. Several authors have recently proven the non-destructive see-through potential of X-ray and neutron computed tomography in the study of corroded coins. X-ray and neutron and scans have been used to clean digitally corroded coin faces (e.g. Adriaens et al. 2010, Nguyen et al. 2011, Bude & Bigelow 2020, Bakirov et al. 2021, Abdurakhimov et al. 2021), extract individual coins from a hoard stored in a clay pot (Miles et al. 2016) or reconstruct coins from the impression they left on corrosion crust after fully vanishing (Warnett et al. 2017). This allowed identification by an experienced numismatist of half of the coins scanned at the most. Scans have also been used to investigate the spatial distribution of remaining alloy and corrosion products (Bozzini et al. 2014, Kichanov et al. 2017, Bakirov et al. 2021, Abdurakhimov et al. 2021) and optimize physical restoration (Bozzini et al. 2014) or reveal the manufacture of coins (e.g. Abramson et al. 2018; Herringer et al. 2018; Salvemini et al. 2018).

2. Materials and methods

2.1. The coins

In **Berlicum** (The Netherlands), one Republican *denarius* (90 BC), 103 copper alloy coins (*asses, dupondii* and *sestertii*) and 3 silver coins (*denarii*) dating from the reign of Vespasian (AD 69–79) to the reign of Marcus Aurelius (AD 161–180) were recovered by metal detectorists. These coins showed intense corrosion and many were covered in thick layers of iron oxides (Fig. 4A,B). Attempts to identify the type and age of the coins by breaking open the concretion was only successful in one third of the cases: These coins could be identified, either by legend and/or by images. Two third of the coins could not be identified as no readable surface was found. Two of these were suspected *subferrati* because of a silvery shine to them, and because they seemed to have been burst from the inside out. Tests by hand-held XRF showed that this

was not the case, but the corrosion processes needed to be further investigated.

Fieldwork to investigate the origin and nature of these heavily corroded copper alloy Roman coins (de Groot & de Kort 2021) yielded two other coins, one of which was used for the present study. This coin was recovered in a trench along the former bed of a small river with upwelling groundwater that flooded regularly. The coin was recovered from a horizon that was rich in nodules of bog iron ore (Fe(III)oxy-hydroxides; see Fig. 3B). Micromorphological study indicated that this horizon consisted of sandy sediment with iron oxide nodules that initially formed around plant roots – probably shortly after deposition – but later were concentrated and potentially somewhat displaced due to erosion and re-sedimentation (de Groot & de Kort 2021). The coin was partially embedded in one of the nodules.

One coin was recovered during excavations in **Krommenie** (The Netherlands; see Fig. 3C), on a roman site. It was probably a watch tower, associated with the 1st century CE Roman fleet base at Velsen (cf. Lendering & Bosman 2012, Driessen 2014, Lange 2021), dating in the first quarter (metal typology) or first half (radiocarbon dating) of the 1st century CE. The site lay on the edge of a gully that connected a coastal peat landscape in the East with the so-called "Oer-IJ" estuarium. At the time, this estuarium was in the final stages of silting up; in the following centuries the landscape became covered with freshwater-peat (Vos 2015). Several coins have been recovered from a gulley-fill that consists of a coarse-grained deposit with large amounts of anthropogenic refuse at this site. When found, the coins were typically embedded in a spheroid concretion of green–blue corrosion materials (Fig. 4C). Breaking open the concretion in order to "read" the coin surface again was in many cases not successful, and in several cases resulted in the coin falling apart: Inside the solid corrosion crust, the coin seems to have been fragmented in thin plate-like fragments. The similarity between this plate-like structure and corroded forged iron led also here to a tentative interpretation of these coins as *subferrati* – although this was not checked with a magnet.

Finally, a coin was incorporated by accident in an oriented micromorphological soil sample from the Roman Mithraeum in **Kempraten** (Switzerland; see Fig. 3D). The Mithraeum was dug into debris of an adjacent former Roman lime manufacture. The central aisle reached down as far as the bedrock, composed of a marl and Nagelfluh conglomerate from the Molasse, on the location of a small spring (ongoing analyses; Ackermann et al. 2020). It is assumed that the building was destroyed at least once if not twice by conflagration. However, newer studies show a probable complex use of the central aisle, where e.g. charcoal and burnt bones seem to have been spread on the floor (Lo Russo et al. 2022). In modern times a lime slaking pit was installed on top of the Roman structure and the area was used as vine yard. The soil sample was taken in the central aisle where layers resulting from occupation, destruction and construction activities are present. Ash residues were only observed in low concentration in the thin section, as they probably dissolved through taphonomic processes (ongoing study; see also Lo Russo 2021, Lo Russo et al. 2022). The coin was lying in a charcoal rich deposit between ample bone fragments and few mortar residues.

2.2. Scanning

The coins from Berlicum and Krommenie were scanned in order to test whether it would be possible to identify the coins, and to preserve detailed 3-D information prior to destructive analyses. For the scanning of the Kempraten sample an impregnated block (4.7 × 4.7 cm and c. 1 cm thick) was available with an excerpt of the coin and its surrounding sediment.

The three coins were scanned using a Nanotom (General Electrics) equipped with a 180 kV X-ray tube and a diamond target at Delft University of Technology (NL). The mCT scanning parameters are listed in Table 1. A brass filter was placed between the source of X-ray and the Berlicum and Krommenie coins to filter out low energy X-rays which would not have penetrated sufficiently the coins and would have

Fig. 3. Locations of and field conditions on the three sites. A: Map with the locations of the three sites indicated. B: Fieldwork at Berlicum. Note the horizon with bleached sand and iron nodules in the profile behind the field archaeologist. C: Field photograph at Krommenie, demonstrating the present wet, organic (reducing) soil conditions. D:: Field photograph at Kempraten, showing the dark layers with ample charred material in the bottom of the trench.

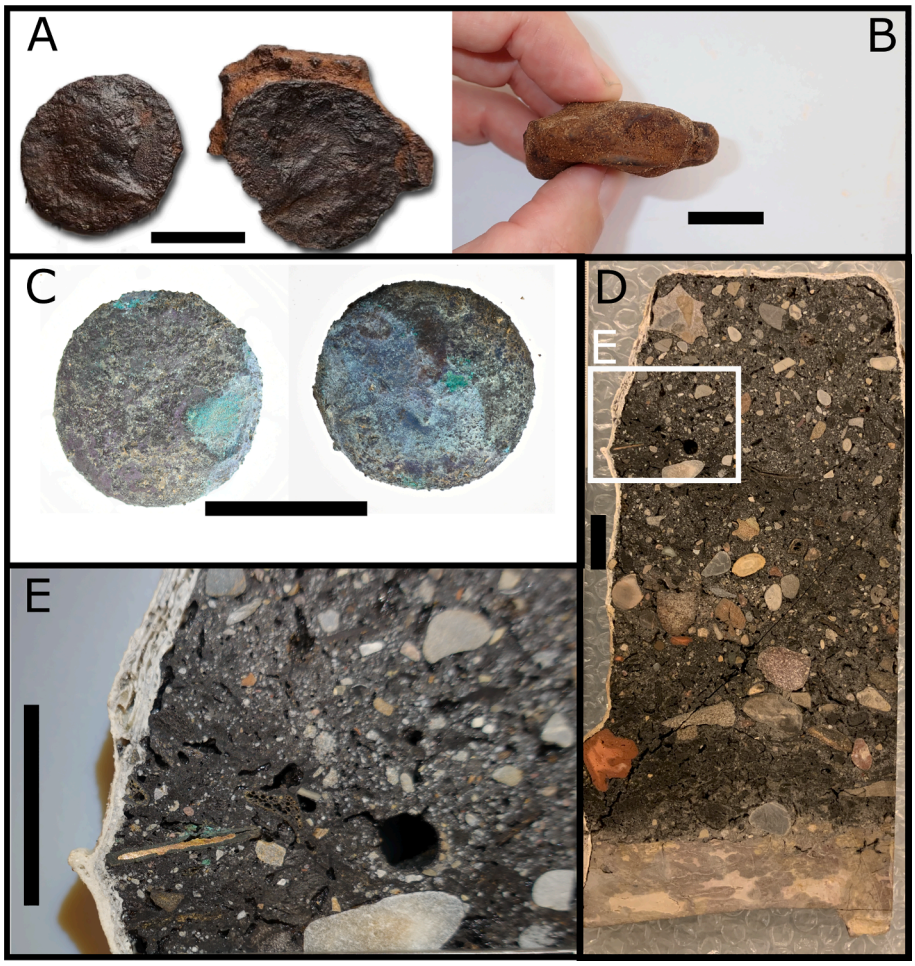

Fig. 4. The objects prior to the analyses. Scale bar = 2 cm. A: One of the coins at Berlicum that was found before the start of the fieldwork. Cracking it open in this case allowed the identification of the coin as an As of Titus. (Image Wim van Schaijk, reproduced from de Groot & de Kort 2021). B: The concretion with coin that was recovered during the fieldwork at Berlicum. C: The concretion with coin from Krommenie. The blue/green colours may have formed after it was excavated. D: Thin slice of the impregnated block of soil with plaster edge from Kempraten. The charcoal rich deposit is visible as dark layer with embedded stones and bones above the bedrock. The area of 4E is indicated in white. E: Detail of 4D, showing the coin embedded in a charcoal rich deposit. A metallic core with green-grey corrosion layer can be observed at the edge of the sample. (For interpretation of the references to colour in this figure legend, the reader is referred to the web version of this article.)

Table 1
X-ray mCT scan parameters.

	Berlicum	Krommenie	Kempraten
Scan type	detailed	full	full
Source mode	0	0	0
Voltage (kV)	170	160	120
Amperage (mA)	0.230	0.09	0.230
Filter material/ thickness in mm	Cu, thick?	brass, x	None
Distance source-object	75	65	90
Distance source- detector (mm)	300	250	252
Voxel size (mm)	0.0125	0.013	0.030
Number of slices	1440	1440	1440
Exposure time (ms)	500	500	500
Number of stacked images	4	5	4
Number skipped images	1	1	1

rendered the edges of the coins brighter or caused streak artefacts around denser parts. The coins were mounted at a tilted position to avoid loss of details that would have occurred if the head and tail faces of the coins would have been parallel to the X-ray beam. Only a part of the Berlicum concretion centred on the coin was scanned to image the coin with a high resolution.

The scanned objects were reconstructed using StudioMax, 2.0 (Volume Graphics) back-propagation algorithms and beam hardening correction filter. The output of the mCT scans was subsequently processed using AVIZO 2020.4. Denoising using anisotropic diffusion and sharpening with a deblur filter were applied to the orthoslices. Slices parallel to the main planes of the coins and 3-D models were created in order to attempt identification of the coins, and to study corrosion phenomena.

The Berlicum coin was also scanned on the FISH neutron tomography beam line of the TU Delft by taking 500 transmission images which serve as input for the tomographic 3D reconstruction model. The resolution of the model is approximately 0.15 mm as described in Zhou et al. (2018). The neutron scans are less detailed than the mCT scans but less affected by X-ray metal artefacts. X-ray CT (mCT) and neutron CT (nCT) were combined to exploit their complementary sensitivities. The mCT instrument provides higher spatial resolution than nCT and its sensitivity scales with the electron density of matter. Neutron CT is complementary in that metals are transparent while light elements like H, Li, B, Cl are well visible in such a matrix of metals.

See Supplementary Information A1,2 for a discussion on comparisons between mCT and nCT scans.

2.3. *Sample preparation*

The samples from Berlicum and Krommenie were impregnated with a polyester resin (ortho Norsodyne O 12,335 AL; Mctechnics). The samples were then cut with a diamond wire saw (0.35 mm) (DWS 250: Diamondwiretech GMBH), and polished. A thin section was produced from the Berlicum sample. This was only partially successful, as the remaining metal core of the coin came loose from the base glass, but the corrosion layers and the concretion were included and could be studied. The thin section is described in de Groot & de Kort (2021). No thin section was made of the Krommenie coin, as it was clear after cutting that the groundmass consisted of sulphides. These minerals are opaque in transmitted light so there was no added value from making a thin section for transmitted light study.

The Kempraten undisturbed soil sample M265 of ca. 10 × 26 cm was impregnated with a polyester resin (based on Araldit DY 026 SP and Laromin C260) under vacuum. Once indurated it was cut in different, around 1 cm thick thin slices (Fig. 4D). Only after this process it became apparent that a coin was also included in the sediment. From the indurated sample one slice was retained for macroscopic study of the samples' cross section. The opposite thin slice was used subsequently to cut blocks (4.7 × 4.7 cm) for the production of thin sections (Beckmann 1997). For the present study, we used the thin slice, the remaining impregnated block and the corresponding thin section (M265.2).

2.4. Optical analyses

The block samples were first studied using low-magnification binocular microscopes with incident light. The thin sections (Berlicum and Kempraten) were studied using polarization microscopes with magnification of 25 – 500 × in plane polarized light (PPL) and with crossed polarizers (XPL). Subsequently, the block samples from all three sites were studied and analyses with the SEM-EDX at the Cultural Heritage Agency lab in Amsterdam. The instrument used is a JSM IT7000HR from JEOL, coupled to a JED-2300-Fully integrated JEOL EDS system (100 mm2 Silicon Drift Detector). Some of the SEM-EDX results of the Berlicum analyses are reported in de Groot & de Kort (2021).

3. Results

3.1. Scan results

Scan results of **Berlicum** coin are given in Fig. 5. In the vertical and horizontal cross-sections of Fig. 5A,B the core of the coin is recognizable as a rectangular homogeneous band in the more heterogeneous encrustation. The concretion has some features that seem root-derived

Fig. 5. Scans and interpretation of the Berlicum coin. A: Cross-section of the concretion with the coin visible as darker (i.e. less attenuating to neutrons), more or less rectangular shape. Scale bar = 10 mm. B: Cross-section parallel to the coins' surface, showing the homogeneous metallic core of the coin and the heterogeneous surrounding concretion, with some suggestion of biological (root-derived) shapes (arrow). C: Equivalent cross-section in (X-ray) micro-CT scan. Note that in this scan the coin is lighter (more attenuating copper alloy) and the concretion darker (less attenuating iron hydroxides). The attenuation of a corrosion pit in neutron and X-ray based scanning (marked in B and C with a light grey triangle) is not fully explained. D,E: Cross sections at the transition of the coin and the concretion, parallel to the surface (D is mirrored). F,G: Possible interpretations of the pattern in D as seated Roma (F) or Securitas (G). H,I: Obverse of coins in F,G: Emperor Hadrian. Image E,F, G,H: American Numismatic Society Public Domain images retrieved 10–01-2022 from numismatics.org; ANS 1906.236.315 and ANS 1987.17.16.

(arrows in Fig. 5A); root tissue was also observed in a thin section of this concretion (de Groot & de Kort 2021). Fig. 5C shows the same cross-section as in Fig. 5B, but in a X-ray mCT scan. Comparing 5B and C shows local differences in X-ray and neutron attenuations, which can give a clue about the chemistry of the corrosion products. The coin shows up in light grey on the mCT and in dark grey on the nCT scan. Corrosion pits also appear in opposite colours (dark grey on the mCT, light grey on the nCT), all except a corrosion pit indicated with a triangle. This deep pit is barely visible on the nCT image while it has a dark colour on the mCT and contains a string of rounded nodules. Cross-sections at the level of the coin surface show some patterning that is probably related to the surface topography and maybe lettering of the coin (Fig. 5D,E). A linear feature and patterning could be a seated figure, e.g. seated *Roma* or *Securitas* (Fig. 5D, F,G), although the patterning may as well be formed by corrosion pits. On the reverse side of the coin, corrosion is less developed and a vague outline of an emperors' head can be distinguished (Fig. 5E). The stamped head presents a X-ray attenuation which is strongly contrasting with that of the crust, allowing a 3D volumetric of the head (see Supplementary information B) and a tentative attribution of this *sestertius* to Hadrian (Fig. 5D,G,H).

Some mCT scan results of the **Krommenie** coin are given in Fig. 6. The oblate spheroidal coin presents different layering patterns. Its core consists of subparallel slightly undulating white and grey laminations (Fig. 6A). The white bands have attenuated X-ray more; they are made of a denser material or a material richer in chemical elements having a high atomic number. Some fissures run parallel to the laminations and are

Fig. 6. Krommenie coin scans. A: mCTscan based cross section through coin centre, showing that the object consists of a stack of laminae surrounded by a massive, layered crust (Scale bar = 5 mm). B: Two cross-sections at the heads end of the coin, showing the outline of an emperors' head. C: Example of emperors head (Augustus). D: Cross-section of the coin at the tail's end. A very vague "SC" may be spotted. E: Tentative outline of the "SC" in D. F: Tails side of the coin in C, showing an example of "SC". G: Photograph of the object. Although vaguely, an "S" (but not the "C") and a countermark with "CAE[SAR]" may be spotted. H: Tentative outline of the "S" and the countermark "CAE" within a square. I: Example of "CAE"-countermarked Augustean "SC" coin. C,F: American Numismatic Society Public Domain images retrieved 10–01-2022 from numismatics.org; ANS 1906.236.315 and ANS 1987.17.16. I: Image copyright Andreas Pangerl, from www.romanscoins.info (cmk-CAE-145a), reproduced with permission (retrieved 10–01-2022).

partially occupied by a discontinuous white material. A thick crack surrounds the stack of laminations. At some points, it bifurcates, becomes more diffuse and even disappears. A second thick crack has initiated from the edge of the coin at a more outward position than the first crack. It vanishes as it propagates towards the dome of the spheroid. It can be seen that only one of the main faces of the laminated core is covered by a thick low attenuating material. Elsewhere the outside rim of the coin is more attenuating and presents a convoluted layering that encapsulates the laminated core. While the outer part of the coin rim is massive, its inner part is dissected by a network of thin polygonal cracks.

Horizontal cross-sections on one side (Fig. 6B) show the outline of an emperors' head, that would match best with emperors like Augustus, Tiberius, Caius or Claudius (e.g. Fig. 6C). However, the head figure is located deep inside the coin therefore cannot represent the surface topography. It is more likely to result from the irregular crack pattern around the laminated core, that may or may not reflect the surface topography.

The other side may show some features related to the reverse sides' image, tentatively identified as showing the letters SC in the central field (Fig. 6 D,E; Fig. 6F as comparison). The letters appear outside the laminated material, but far from the coin surface, again in a zone which may have been deformed by expanding material. The "S" of the "SC" seems also to be visible at the surface of the concretion (Fig. 6G), with a countermark, possibly CAE(SAR); cf. Fig. 6H. This would make it an Augustan coin (moneyers' *as*), minted between 16 and 2 BC, countermarked around 15–20 AD. Such coins have also been found at Velsen fortress close by (Bosman 1997) and would be in line with its abandonment after 28 AD and with the dating of the Krommenie-site in the first quarter or first half of the first century AD.

The mCT scans demonstrate that the **Kempraten** coin is only a small fragment: most of the coin has been lost during the thin section preparation process. The scan of the complete impregnated block (not shown) illustrates the heterogeneity of the soil surrounding the coin: next to the coin, sand grains, bone and teeth fragments as well as charcoal fragments could be identified. The detailed scan reveals the inner structure of the coin. A small (1.6 mm long, only 0.18 mm thick) segment of uncorroded core is preserved in the centre of the 1.1 mm thick coin fragment as a homogeneous area with very high attenuation. The mCT scans (Fig. 7) give a diverse picture: A small segment of uncorroded core is preserved in the centre as a homogeneous area with high attenuation. The rest of the coin shows a large proportion of irregular cavities or fissures and a heterogeneous groundmass: It has a background of low attenuations, in which irregular dendritic domains with high attenuation occur throughout. The outer rim of the coin forms a zone of intermediate attenuation intersected by numerous radial cracks. Because a layer of corrosion products or concretion is lacking, it was possible to segment and 3-D render the original surface of the coin. This 3-D construction produced rows of round dots on the surfaces on both sides of the coin. It also allowed to determine the diameter of the coin at about 14.5 mm. It was not possible to identify the coin, but most probably it is either an Antoninianus (radiate) of the late 3rd century CE or a bronze coin of the first half of the 4th century CE.

3.2. *Cross sections studies*

In this section, we report for each coin on (1) the incident light observations of the block samples, (2) the thin section analysis (if available) and (3) on the SEM-EDX observations and measurements.

3.2.1. *Berlicum*

In incident light (Fig. 8A,B), the cross-section of the Berlicum concretion clearly shows an uncorroded core of the coin. The surrounding corrosion layer is massive, but has heterogeneous colours ranging from red and orange to black. Black material seems to be more prominent near the coin's surface. The distribution of the colours especially in the rim-area, suggests that the original surface of the coin was in what is now the concretion. It seems that the coin used to extend several mm from the present rim of the uncorroded core, a part that now seems to be replaced by the concretion material. Apparently, the corrosion happened anisotropically: little corrosion from the surface, but strong from the rim of the coin inwards. Sand grains are embedded in the concretion material, but this is not apparent everywhere.

Few observations could be made on the thin section: the coins' core is opaque (and came loose as it did not adhere to the base glass), as is the red–orange-black cement. One point of interest was the observation of remnants of a plant root that was embedded in the concretion (Fig. 8C).

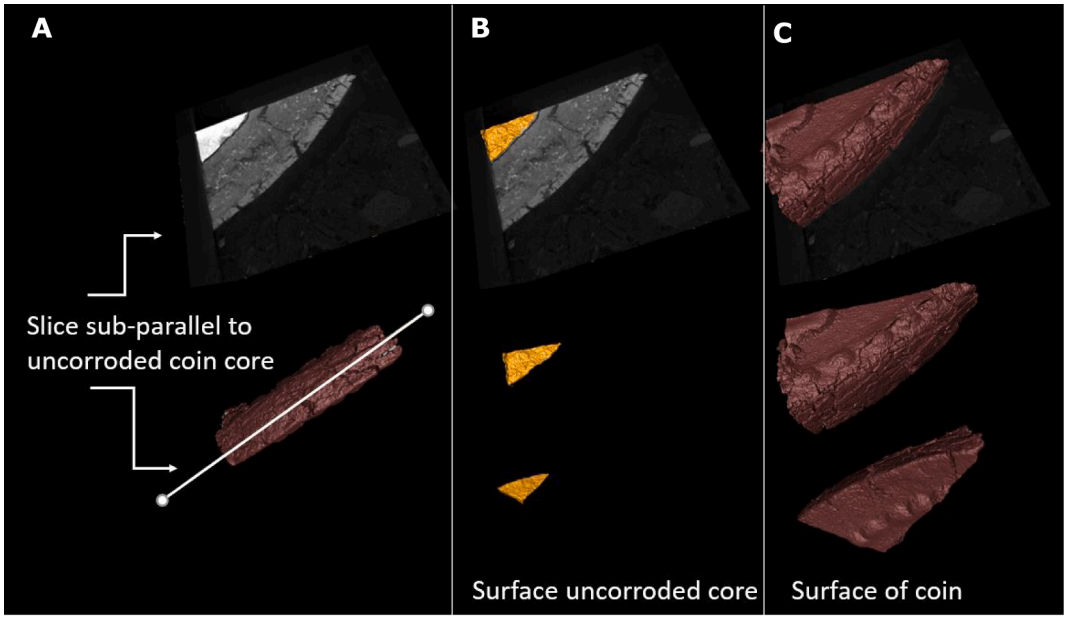

Fig. 7. Results of the mCT scan of the Kempraten coin fragment that is embedded in the impregnated soil block. The cross sections (A) clearly show the depleted outer rim with fissures and the metallic, uncorroded fragment in the core of the coin. The lack of corrosion crust made it possible to 3-D render the coin's surface (C) as well as other features, like the metallic uncorroded core remnant (B). The coin's rendered surface shows that the coin had a row of rounded dots near the edge. The fissuring at the rim is also apparent.

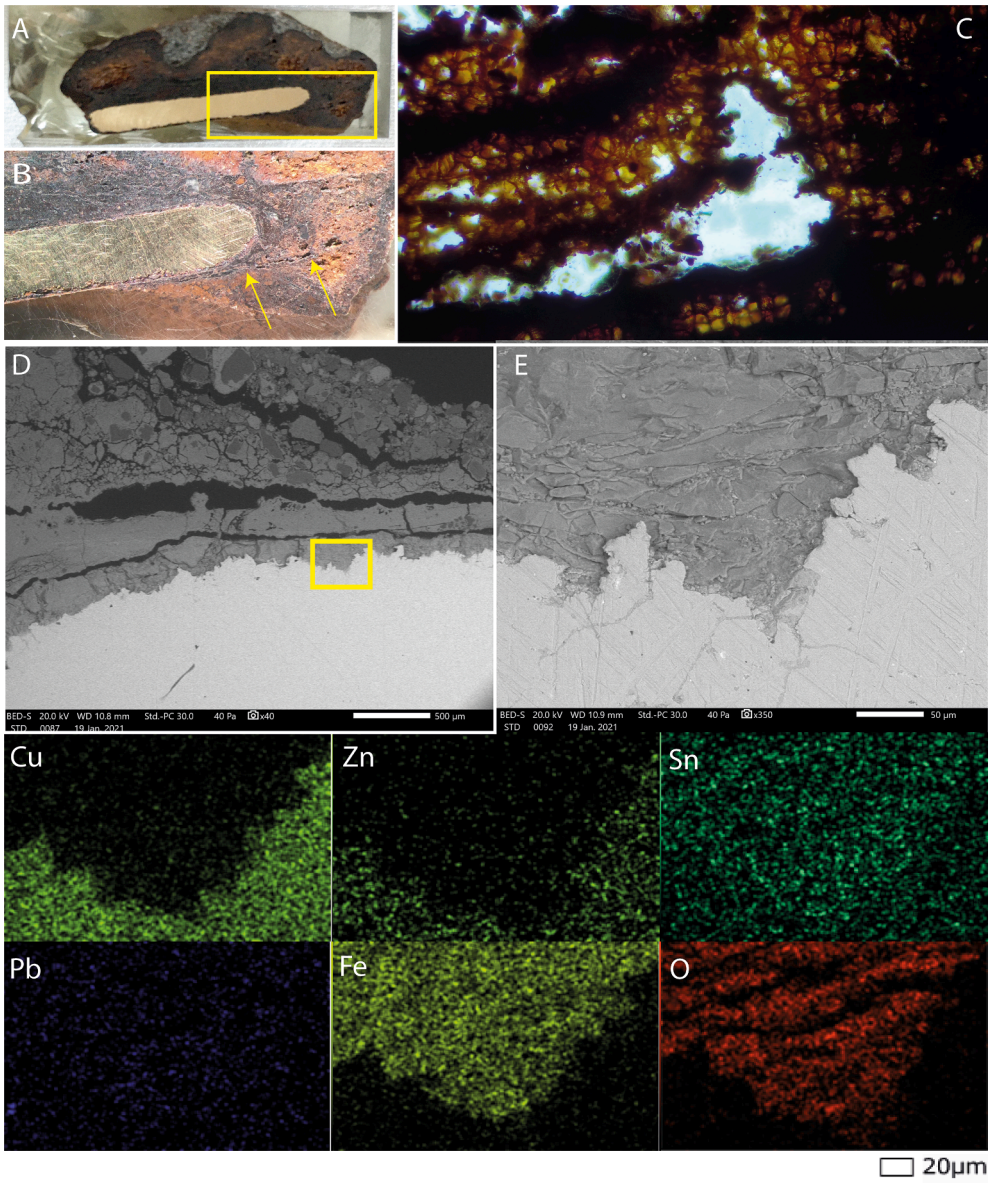

Fig. 8. Berlicum coin cross-section analyses. A: Cross-section through the concretion, seen with incident light. The uncorroded core of the coin is clearly visible. The yellow-lined square indicates the area in B. B: Detail of coin core in concretion, showing the colour-variation in the concretion. The arrows indicate the original surface of the coin. C: Microscope image (transmitted plane polarized light) from the thin section with root tissue in the concretion. D: Backscatter (BE) image of the contact between the core (light grey) and the surrounding concretion (darker grey), showing a sharp, irregular boundary. The concretion is banded and shows fissures and cavities (black). Close to the coin, the concretion is massive and homogeneous, but the outer regions are more irregular with embedded sediment grains. The yellow-lined square indicates the area in E. E: Idem, detail of the core-concretion contact with element mappings. Cu and Zn are mostly restricted to the uncorroded metallic core, whereas the concretion is dominated by Fe and O. Note that the distribution of Sn is similar in the core and the concretion, as is the presence of minor amounts of Pb. F: BE image of another part of the concretion within the original coin volume, showcasing the distribution of Sn and other components. Note in F the pattern of light grey-white convoluted bands in the top, and parallel bands in the lower part of the image. Yellow-lined squares indicate the areas in G, H, I. G: BE images and element mappings of G; the light-grey features in the top of the image are sn-rich, whereas the white–grey clusters in the lower half contain Cu and S. H: Idem, showing thin parallel sn-rich bands, enveloping an elongated Cu-dominated feature. I: Spherical features dominated by S, with Cu in the core and an outer skin with Ag.

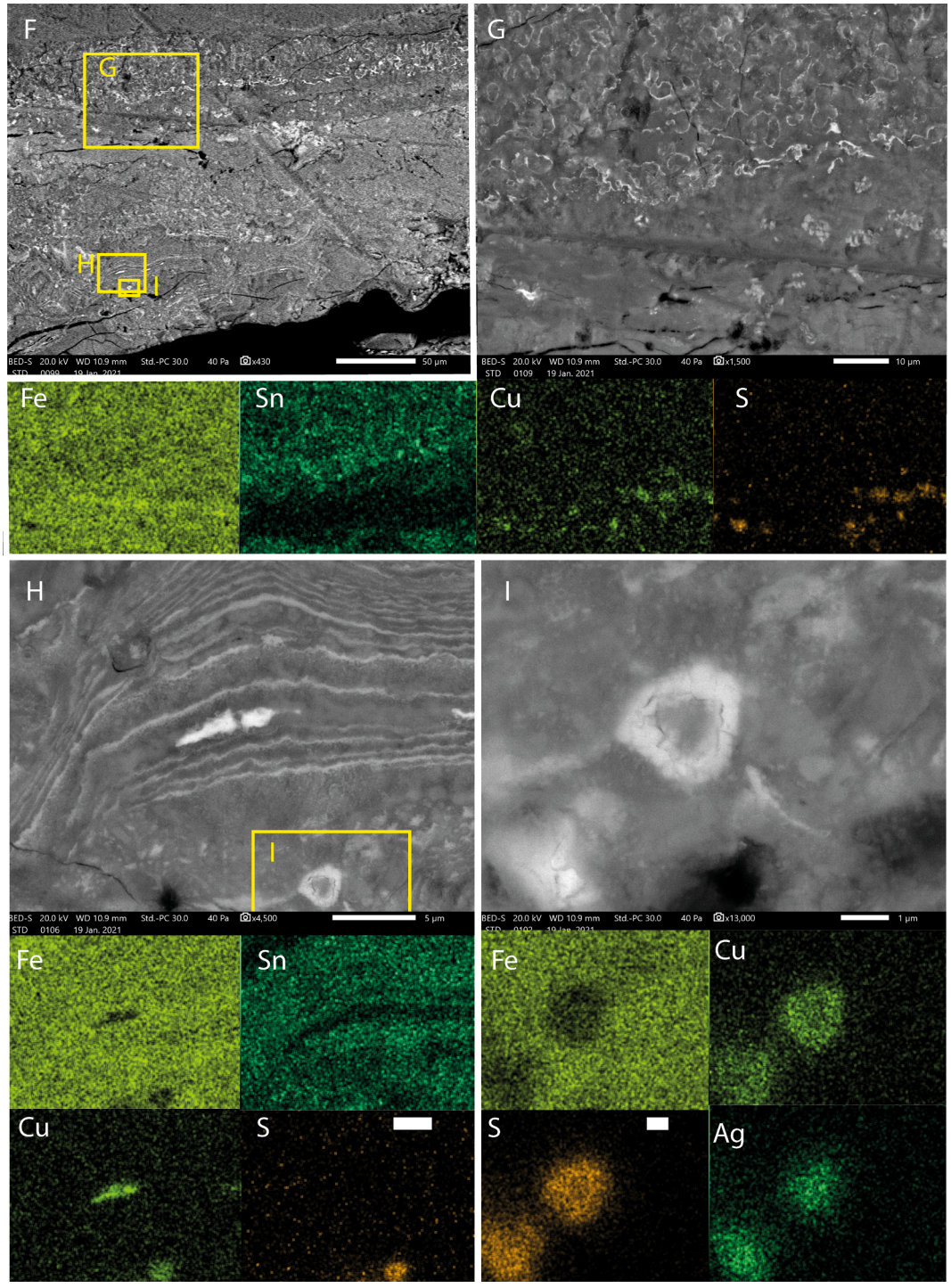

Fig. 8. (*continued*).

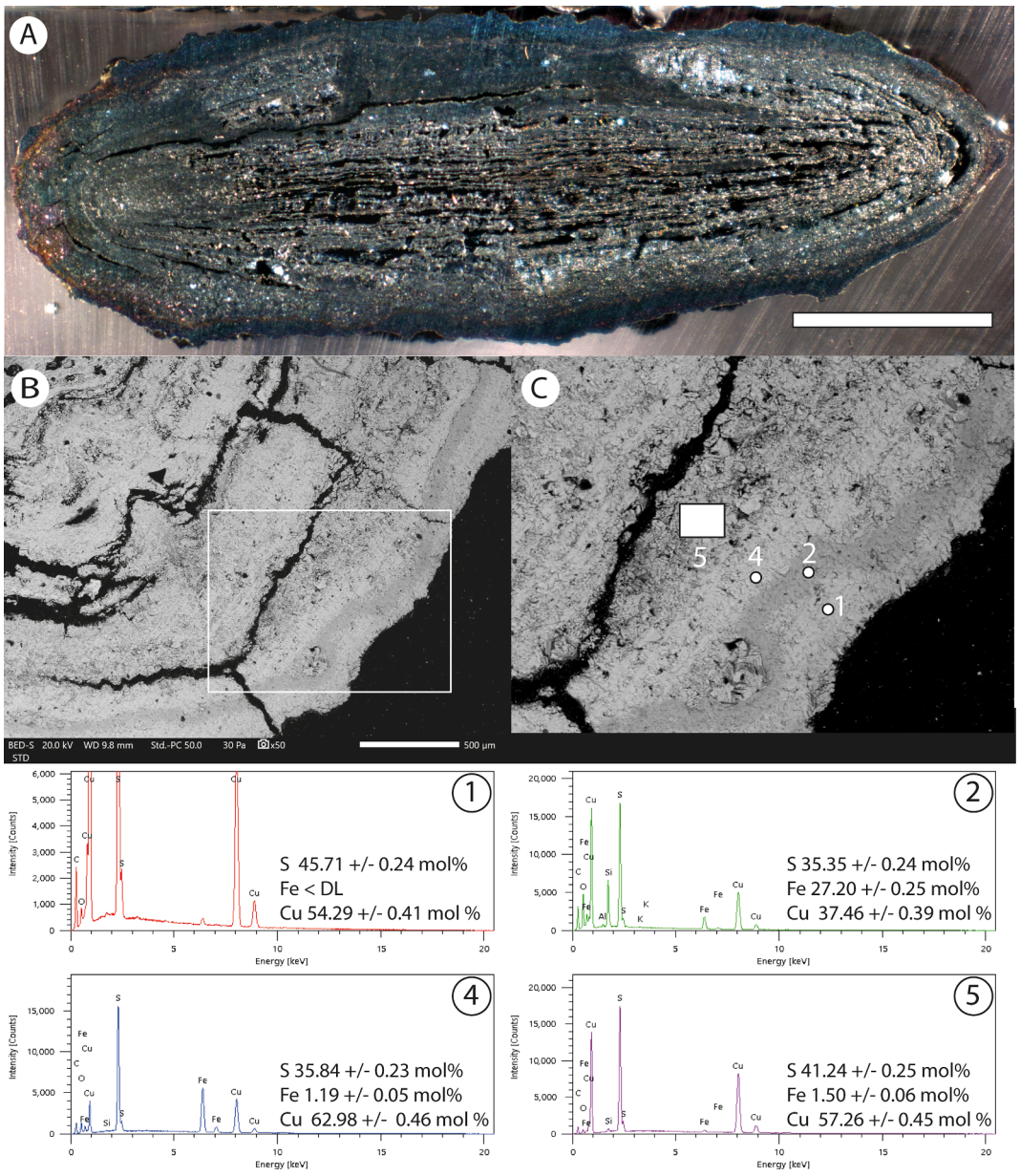

Fig. 9. Krommenie coin concretion cross-section analyses. A: Cross section of the Krommenie coin with incident light. The thin separate laminae in the core with a grey-metallic colour are clearly visible. The massive outer crust includes a blueish band. (Scale bar = 5 mm) B: BE image of the concretions' surface. Note the banded, massive nature of this part of the concretion. The square indicates the area of C. C: Detail of B and accompanying EDX-spectra. Spectrum positions are indicated with dots (spot measurement) and a square (area measurement). The groundmass consists of copper sulphides (probably a mix of CuS and Cu_2S; covellite and chalcocite) with traces of iron (<2 wt% Fe), but the dark band parallel to the surface (measurement 2) contains much more iron. D: BE image from the transition of the solid surface to the laminated core of the coin. E: As D, overlain with S and Cu element mappings. Banding with higher and lower S contents are apparent. F: Core of the coin, showing the stacking of very thin (<10 – 100 µm) lamellae. The area of G is indicated. G: Detail of F (turned 90°) with associated element mapping. The area that is mapped is indicated by the yellow square. Dark grey lath-shaped minerals are embedded like phenocrysts in the light-grey massive groundmass, forming a porphyric structure. The element maps show that these minerals are calcium sulphates, i.e. gypsum or isomorphs embedded in copper sulphides. In addition, the map of S shows banding at this level as well.

Backscattered electron (BE) images (Fig. 8D,E) show a sharp, irregular boundary between the uncorroded core and the iron oxide-dominated concretion. Element mappings confirm the metallic nature of the core (no O), which consists of a leaded Cu-Sn-Zn alloy. In the Fe,O dominated concretion, Cu and Zn concentrations are very low/absent, but the distribution of Sn and Pb seems unaffected. In more detail, however, as in Fig. 8F-I, it becomes clear that the Sn compounds in the concretion within the original coin volume are distributed in thin parallel or convoluted bands – probably as SnO_2 – embedded in the Fe(III) oxide groundmass. Apart from the tin oxides, small (micron to sub-micron scale) inclusions can be observed of remnant metallic Cu (Fig. 8H), Cu,S compounds (Fig. 8G) and – in one case – a combination of Cu,S and Ag,S compounds (Fig. 8I). The concretion outside the original coin volume does not contain Sn, but Cu-rich bands are embedded in the iron oxides (Supplementary Information).

3.2.2. *Krommenie*

In cross-section, the Krommenie coin is dark grey to metallic in colour. The outer shell of the concretion is massive, but – as was already demonstrated by the mCT scans –- the coins' core consists of a series of

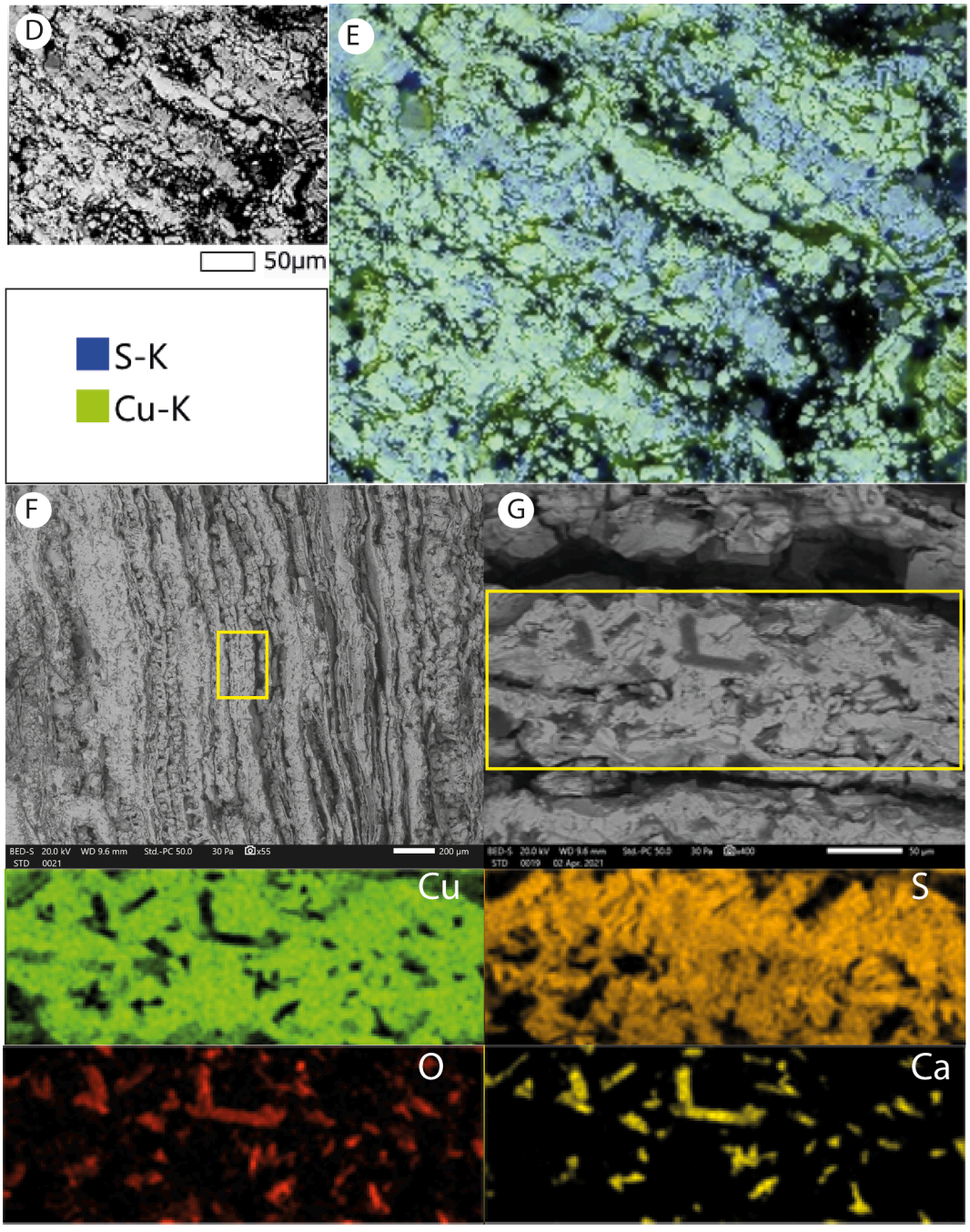

Fig. 9. (*continued*).

thin parallel lamellae, separated by elongate cavities, giving it an overall appearance of a stack of thin slivers of dark material. A metallic blueish band is visible in the outer shell. It is not clear from the cross-section whether the original surface of the coin is still present in the concretion (Fig. 9A).

BE images at the surface of the concretion show that this massive layer still shows some layering (Fig. 9B,C). Point and area measurements show that the groundmass throughout the object consists of Cu,S compounds with composition varying between CuS and Cu_2S end members. Iron is incorporated in the surface layers only, mostly concentrated in a conspicuous band with unclear mineralogy parallel to the surface. (Stoichiometrically, with Fe 27 mol %, Cu 37 mol% and S 35 mol% - recalculated from the weight percentages; the S concentrations are too low for all the iron to be present as chalcopyrite). This probably correlates with the blueish band that is visible in incident light in Fig. 9A). In the transition to the core, the laminated patterns become more prominent, and it becomes clear that S-rich zones occur in zones parallel to the laminations (Fig. 9D-G). In the core of the coin, the Cu,S laminae incorporate large euhedral Ca-sulphate minerals, most likely gypsum.

3.2.3. *Kempraten*

The incident light observations on the block (Fig. 10A,B) show how the coin is embedded in an anthropogenic deposit with ample debris and charred material. A remaining metallic core of the coin can still be seen, as well as some remnants of green corrosion products (probably malachite; $Cu_2CO_3(OH)_2$) in the surrounding soil. In the thin section (Fig. 10C,D) ample charcoal as well as large bone fragments can be

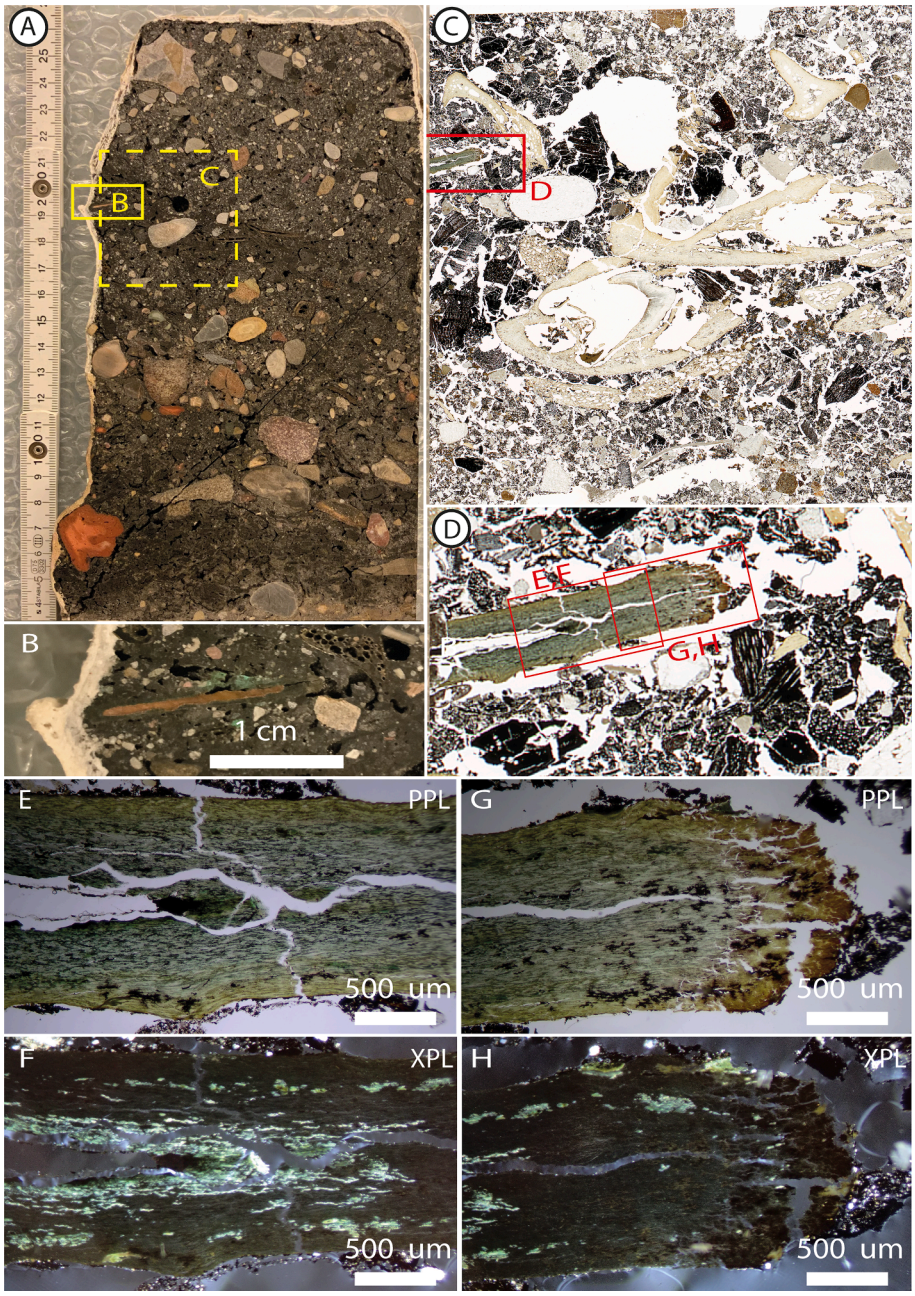

Fig. 10. Observations of cross-sections through the Kempraten coin. A: Photograph of the impregnated block in which the coin was embedded. Yellow boxes show the positions of B and C. B: Enlargement of A, showing the coin embedded in the block. The uncorroded metallic core is apparent, as are some remnants of green corrosion products in the soil surrounding the coin. C: Scan of the thin section with embedded coin, with visible bone fragments and charcoal. The box indicates D. D: Enlargement of C, showing the coin in the thin section. Note that the metallic uncorroded core is missing in this sample. Boxes indicate E-H. E: Plane Polarized Light (PPL) micrograph of the centre of the coin, surrounding the cavity where the uncorroded core was. The groundmass of the coins is banded green with some irregular black-opaque inclusions. Near the surface of the coin, the colour is more yellow. F: Idem, with crossed polarizers (XPL). Most of the groundmass shows very little birefringence, apart from the zone immediately surrounding the core, and smaller elongated domains throughout the groundmass. G, H: PPL and XPL micrographs of the edge of the coin. Although similar to E and F, the very edge of the coin shows considerable fissuring, and colours that go from yellowish to brown. I: BE image and mappings of the uncorroded core and surrounding area. The corroded area is strongly depleted in Cu, but Cu values are a bit higher in the zone immediately next to the core. The edge of this zone is formed by light irregular domains that are rich in Ag and S. Pb occurs throughout the groundmass – its apparent lower concentrations in the core is an artefact of the higher Cu concentrations there. Thin bands parallel to the coin's surface show elevated Cu and O. J: BE image and mappings of the edge of the coin, showing clearly the wider fissures at the coins' edge. This zone is richer in Sn, but the mapping shows some small domains richer in Cu (and O; not shown) as well. The Pb mapping shows a thin band in the lower right corner.

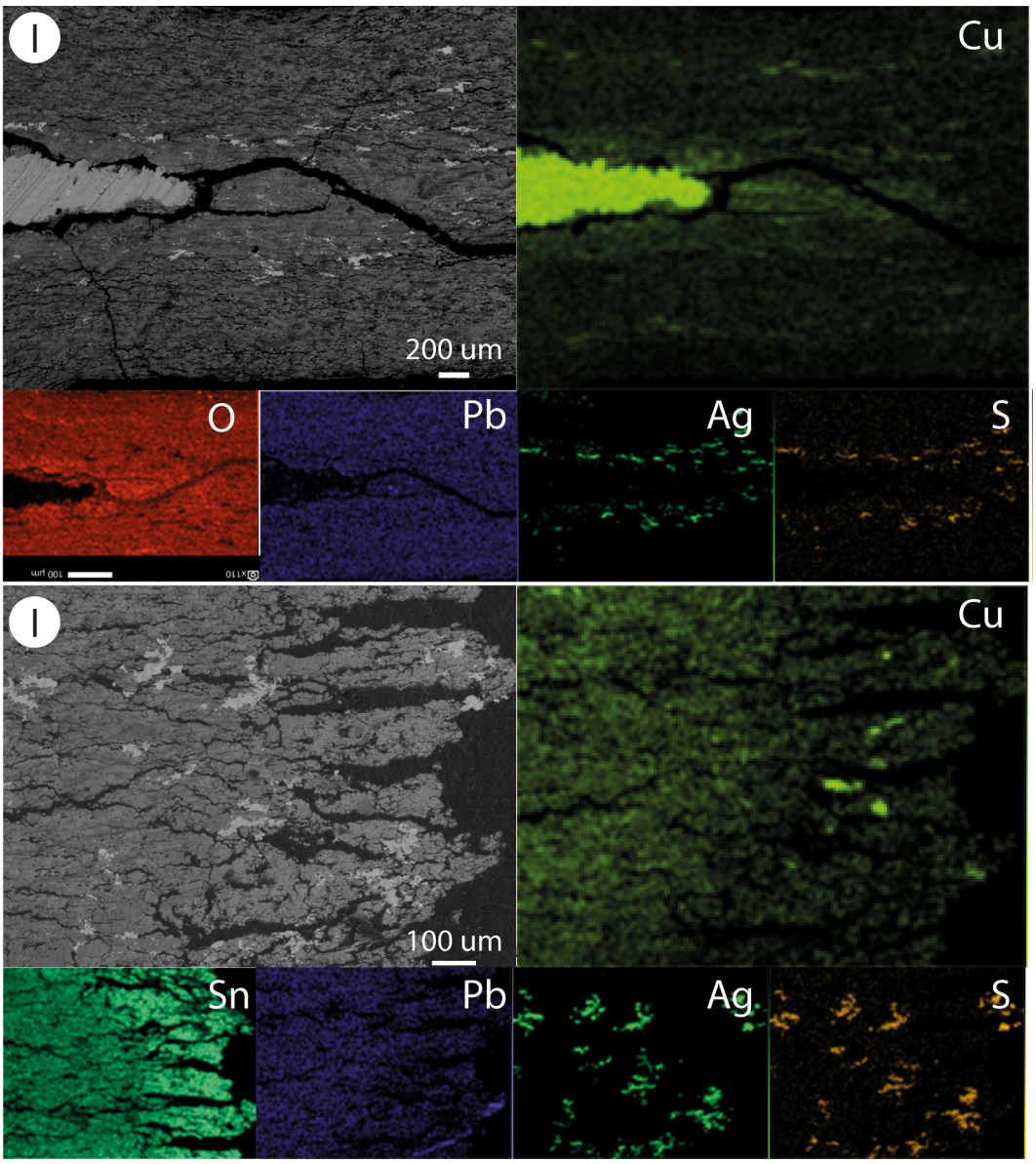

Fig. 10. (*continued*).

observed. The metallic core was not incorporated in the thin section as it probably (like in Berlicum) did not adhere to the base glass plate. Surrounding the uncorroded metallic core, the corroded part of the coin in PPL consists of a green groundmass with banding parallel to the coin's surface. No corrosion products were apparent in the soil surrounding the coin in the thin section.

The micrographs in PPL (Fig. 10E,G) show that the green banded groundmass in the coin changes to more yellow colours at the edge, and even towards brown at the rim of the coin. Embedded in this groundmass are opaque irregular mineral features. They seem to occur preferentially in bands. The rim of the coin is strongly fissured, with V-shaped voids, as was already indicated based on the mCT scans. XPL micrographs (Fig. 10F,H) show in general that the groundmass of the coin is hardly birefringent, except for (1) the material immediately next to the uncorroded core and (2) isolated elongated domains parallel to the coins' surface. The green PPL colour and – in XPL - strong birefringence identify these as domains of malachite. There are no indications of the occurrence of tenorite. This mineral has a distinct light to dark brown colour, a strong blue to grey anisotropism and is weakly pleochroic (mindat.org).

SEM-EDX analyses show that, compared to the uncorroded core, the green banded groundmass is strongly depleted in Cu (Fig. 10I, 11). The malachite-zones identified in thin sections seem to appear in the SEM-mappings as zones with slightly higher Cu and O concentrations in the Cu-depleted groundmass. The opaque irregular mineral features spotted in the thin section appear in the SEM images (Fig. 10I,J) as light grey irregular Ag,S inclusions. It is remarkable that there seems to be a concentration of Ag,S inclusions at the outer edge of the malachite-dominated zone (Fig. 10I). At the coins' rim, the fissure-rich zone has even higher Sn-concentrations than the rest of the Cu-depleted mass. Fig. 11 shows that whereas the uncorroded core has Sn concentrations around 5 %, they rise to ca. 20 % near the core and approach 40 % close to the rim of the coin, while Cu concentrations drop from ca. 95 %, to ca. 20 % near the core and < 10 % close to the rim. The lead mapping (Fig. 10J) makes a faint band of increased lead concentrations visible on the outside of the coin near the rim. Point measurements in this band confirmed increased lead concentrations on the corroded coin, but a pure lead phase could not be discerned.

The corroded Sn-rich material contains elements that are not present in the uncorroded core: Most noteworthy are Ca, P and As. (See Table 2).

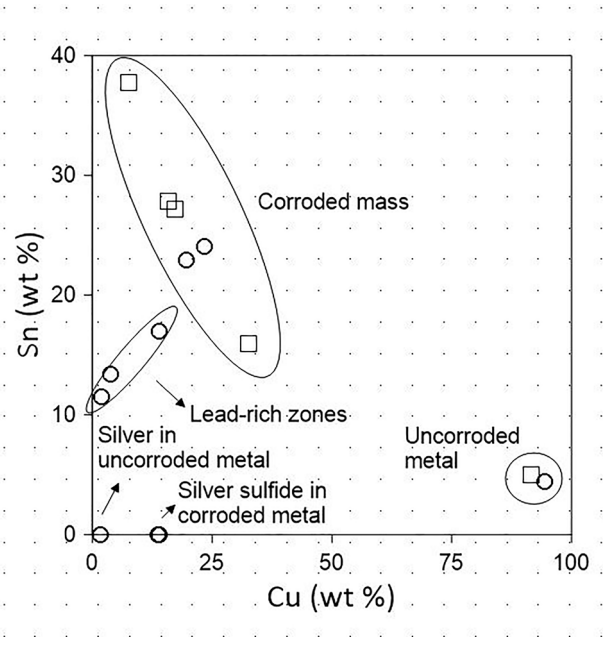

Fig. 11. Cu, Sn concentrations from spot- and area measurements on the Kempraten coin. Indicated are measurements from the uncorroded core, corroded material, Pb-rich material and Ag-rich inclusions on both the uncorroded core and the corroded material. Circles are spot measurements; squares are area measurements.

Table 2
Selected element concentrations of SEM-EDX measurements on the Kempraten coin. The complete dataset is in Supplementary Information C. Note that the C and O concentrations may be affected by the resin with which the sample was impregnated.

Measurement nr.	Measurement type	Location in coin	C	O	S	P	Cl	Ca	Fe	Cu	As	Ag	Sn	Pb
Spc_001	Spot	Ag, S inclusion in corroded groundmass	17.82	7.68	6.94	0	0	0.9	0	1.73	0	64.4	0	0
Spc_002	Spot	Lead-rich band in outer corrosion layer	30.52	27.9	0	1.59	0.76	1.64	0	3.95	0	0	13.41	19.57
Spc_003	Spot	Lead-rich band in outer corrosion layer	47.13	22.47	0	0.96	0.5	0.97	0	2.05	0	0	11.47	10.2
Spc_004	Spot	Ag inclusion in uncorroded metal core	11.17	15.22	0	0	0	0	0	13.89	1.75	57.41	0	0
Spc_005	Spot	Ag inclusion in uncorroded metal core	8.13	9.39	0	0	0	0	0	13.82	0	68.3	0	0
Spc_006	Spot	Uncorroded metal core	0	0	0	0	0	0	0	94.45	0	1.09	4.46	0
Spc_007	Spot	Inclusion in uncorroded metal core	27.44	10.2	0	0	0.23	0	0.13	56.7	0	0.76	3.15	1.04
Spc_008	Spot	Inner corroded zone	0	38.86	0	1.74	0	1.21	0	23.33	0	0	24.1	9.49
Spc_009	Spot	Inner corroded zone	26.75	25.28	0	1.39	0	1.1	0	13.88	0	0	16.97	8.54
Spc_010	Area	Outer corroded zone	0	41.33	0	2.08	0	1.36	0	19.69	0	0	22.89	11.29
Spc_011	Area	Uncorroded metal core	0	0	0	0	0	0	0	91.55	0	1.3	5	2.15
Spc_012	Area	Inner corroded zone	0	39.27	0	1.23	0	0.78	0	32.6	0	1.67	15.98	8.47
Spc_013	Area	Outer corroded zone near rim	0	43.11	0	0.7	0	2.09	0	7.61	0	0	37.77	6.79
Spc_014	Area	Outer corroded zone near rim	0	49.07	0	0	0	1.75	0	15.76	2.78	0	27.85	0
Spc_015	Area	Outer corroded zone	0	48.67	0	0	0	1.56	0	17.3	2.93	0	27.15	0

4. Discussion

4.1. Original coin composition

The original composition of the Berlicum and the Kempraten coins could be determined on the uncorroded metallic core: The Berlicum coin was made from a Cu-Zn-Sn alloy (tin-containing brass or *orichalcum* or gunmetal). The Kempraten coin was made of a low-tin bronze, but with small domains of lead and of silver scattered through the alloy – a common feature in coins from this period. No uncorroded material was left in the Krommenie coin, so we cannot be sure about its original alloy composition.

4.2. Copper corrosion in terrestrial gley zones: Berlicum

The corroded copper alloy coin from Berlicum represents copper alloy objects that have become buried in gley zones: sediments or soil horizons with accumulated iron(III)oxides due to fluctuating iron containing groundwater levels (see Appelo & Postma 2004 for the geochemical process). These zones combine alternations between oxic and reducing conditions with relatively low pH dependent on the groundwater level. If fed by upwelling groundwater, iron accumulation can become substantial. Iron-rich upwelling groundwater usually has a bicarbonate (HCO_3^-) buffered system, with pH above 7. However, oxidation of the dissolved Fe^{2+} and the precipitation of Fe(III)

oxyhydroxides causes acid to be released according to the reaction:

$4Fe^{2+} + O_2 + 6\ H_2O <-> 4FeOOH + 8H^+$

The net corrosion processes in these environments can be described as a progressive loss of Cu and Zn from the alloy, which is replaced by Fe (III)oxyhydroxides, where the Sn that was present in the alloy precipitates as SnO_2. Additional Fe(III)oxyhydroxides precipitate in the pores of the sediment around the object, cementing the sediment grains and causing a concretion to form. In the cemented sediment, some of the dissolved Cu from the coin may precipitate again, usually as malachite (copper carbonate). Behind this net result are probably a series of redox processes that alternate between waterlogged (reducing) and dry (oxidizing) conditions, in which pH is influenced by new mineral formation:

Copper alloys dissolve under acidic conditions. In a soil where oxygen is present, copper can corrode and if soil pH not too acidic (usually > 6), basic copper carbonate compounds such as malachite and azurite usually form. These have a characteristic green or green–blue colour. The green copper minerals malachite and azurite are stable from pH 10 to about pH 6. If the pH is lower, these compounds can dissolve again, causing the passive protective layer around the object to become thinner. This is what probably happens in the gleyz ones where iron(III) oxyhydroxide precipitation results in lower pH values: the lowered pH causes passive copper carbonate minerals to dissolve, and then also the metallic copper itself. Dissolving copper carbonate can lead to a pH increase, causing iron hydroxide to precipitate precisely on the surface of the object. In addition, the released Cu^{2+} has a catalytic effect on ferrous iron oxidation by oxygen (Stumm and Lee, 1961). As a result, dissolving the copper will cause a stronger build-up of ferric hydroxide around the object than in the surrounding non-copper-containing sediment.

Tin, like lead, will form an insoluble oxide. Zinc, however, will probably dissolve similar to copper because Zn^{2+} only forms stable zinc hydroxide or zinc carbonate at a pH higher than 7. The SnO_2 seems to form thin laminae (parallel or convoluted; see Fig. 8F-H). It is unclear whether these laminae represent consecutive oxidation episodes. The final effect is that the coins lose copper and zinc, leaving mainly compounds of tin and to a lesser extent lead. The tin and lead content in particular will be strongly increased at the outside, compared to the composition of the coins in the core.

Preferential leaching of copper and zinc from copper alloy objects is a common feature in copper alloy corrosion, and it plays a significant role in discussions on the application of pXRF or other surface measurements in copper alloys (Gigante et al. 2005, Orfanou & Rehren 2014, Roxburgh et al. 2019). However, the role of iron in Berlicum-like burial conditions, and its implications for the composition of the corrosion layer has not been described before.

The presence of some Cu and Ag sulphide species in a specific part of the corrosion layer (Fig. 8H,I) indicates that in Berlicum, some sulphur species have become available during the corrosion process. It is most likely that the sulphide species were already present in the coin when it was manufactured. It is unlikely, however, that these sulphidic compounds have had much influence on the overall progress of the corrosion processes.

4.3. Copper corrosion in coastal settings: Krommenie

It is remarkable that the whole coin of Krommenie has been transformed into corrosion products, with no original uncorroded core left: The coin proper has been transformed into laminae of Cu sulphides in which gypsum crystals are embedded. An outer corrosion crust has formed of Cu sulphides in which some iron is incorporated, and which contains one iron-rich band. The most puzzling feature in the Krommenie coin is the abovementioned embedding of sulphate (gypsum) crystals in the Cu sulphide lamellae in the core of the coin: The co-existence of sulphates and sulphides is already unexpected, as they are stable at different redox conditions. The origin of the Ca is maybe even more puzzling: It must have come from outside the coin, i.e. the burial environment or groundwater, at a moment that corrosion had already caused such a degree of damage to the coin that fissures or cavities had formed. Given the bulk of the evidence, it is likely that the coin's corrosion was the result of either fluctuating or changing burial conditions in a sulphide/sulphate-rich environment:

- Under reducing conditions, Cu oxidation, triggered by sulphate reducing bacteria (SRB) results in the formation of copper sulphides and possibly also copper-iron sulphide minerals.
- During oxygenation events (for example high or low tide) sulphide oxidation in a calcium carbonate rich environment (e.g. shells) may have led to elevated concentrations of Ca^{2+} and SO_4^{2-} in the sediments porewater, and caused the precipitation of gypsum in fissures in the coin. In addition, the formation of sulphate by sulphide oxidation produces H + ions which may facilitate metal attack once more before a new round of SRB attack occurs. These gypsum crystals subsequently become embedded in copper sulphide corrosion products during one or more next reducing phases.

These steps, that may have occurred several times, could result in the observed phenomena, but other sequences of such events cannot be excluded. All, reactions in an alternating anaerobic/ aerobic copper sulphide system are extreme complex as many species and many stable and unstable phases are involved (Little et al. 1991). What is clear, is that the corrosion must have taken place in alternating sulphidic and aerobic conditions, probably also with salty or brackish influence. Moreover the burial conditions cannot have been constant (otherwise a sulphate-sulphide combination would be inconceivable), and it is likely that sulphide-oxidation drove some of the processes. Most important is that the high-energy changing coastal sedimentary conditions were detrimental to the preservation of copper alloys, including the coin that we studied.

If the corrosion processes as described occur, but without the last phase of reducing conditions, the objects may fragment and disintegrate. Focussed research on such occurrences may in future help understand the corrosion patterns that we observed in the Krommenie coin.

4.4. Copper corrosion in charcoal rich deposit: Kempraten

The Kempraten coin was buried in a charcoal rich deposit. Based on the archaeological evidence, we cannot exclude that the coin was affected by a conflagration event. However, no tenorite was observed, so the coin was not heated to temperatures above 300 °C.

The corrosion in the Kempraten coin has progressed further than one would expect in a neutral to basic freshwater burial conditions. One would expect a thin corrosion layer or patina that served as passivation layer, and would protect the unaffected metal from further degradation. In the coin, malachite occurs mostly in a zone surrounding the uncorroded core, and as relict islands in a groundmass that essentially is a Sn-rich amorphous mass. In addition, it is remarkable that of the vast amounts of copper that must have leached from the coin, very few is still present in the surroundings of the coin. In a neutral to basic environment, one would expect Cu precipitation (mostly in the form of malachite) in the groundmass immediately surrounding the coin. The photograph in Fig. 10B shows that some malachite is present in some part of the soil block, but only a small amount compared to what must have leached from the coin. Cuprite has not been observed at all.

Carbonized remains are common in this deposit, but ashes are rare. As mentioned in the introduction, this may be because the calcium- and potassium hydroxides that form major component of wood ash remains are very soluble, and therefore rarely survive outside of e.g. caves. In open air sites, these components will quickly dissolve in rain or percolating groundwater. However, the temporary elevated pH (>12?) that

can be caused by the presence of these hydroxides may result in the dissolution of copper corrosion products; Malachite e.g. is only stable at pH < 11 (McNeil & Little 1999). It is therefore remarkable that the most corroded parts of the Kempraten coin show elevated concentrations of Ca (Table 1). Ashes that were present in the burial environment but have since dissolved and leached may have formed the source for this Ca. Dusty clay coatings that were observed in thin sections in this charcoal-rich deposit may be related to the influence of these ashes on clay stability (cf. Huisman et al. 2012), but this could not be determined with certainty, especially since one would then expect limpid clay coatings.

We therefore think that the corrosion of this coin, with intense leaching, occurred under the influence of the ashes that once must have been present in the burial environment. The high alkalinity will have disappeared over time due to dissolution and leaching of the soluble ash components, leaving only the insoluble carbonized remains. Subsequent corrosion resulted in the net transformation of the outer part of the remaining core from metal into malachite.

It is remarkable that the degree of Cu leached is not homogeneous. Most striking is that the outer rim of the coin has been leached to such a degree that the remaining corroded mass has shrunk, resulting in a pattern of parallel V-shaped fissures. Here, the coin also obtained a more yellow-orange than green-grey colour. It is unclear why this colour change occurred.

The thin band of Pb-rich material in the outer part of the corroded coin is remarkable too: It implies that lead has gone into solution, and later precipitated on the surface of the coin remnant. Like copper, lead oxides can dissolve at high and low pH values; in this case therefore, it is most likely that the lead from the corroded parts of the coin was leached, and that only a remnant precipitated. It is unlikely that modern lead (e.g. from pesticides in vineyards) would leach and precipitate to such a degree that it would be detectable in a corrosion layer.

The distribution of silver compounds is something of a mystery: The silver was originally present throughout the coin. During the oxidation of copper and tin and the leaching of a large proportion of the copper oxidation products it remained more or less in place during the oxidation of copper and tin. However, it seems to have become redistributed during the corrosion process, concentrating on the boundary between the malachite-area and the surrounding tin-rich amorphous core. This would suggest that at least some of the silver got into solution and was transported towards the core, where it precipitated on contact with malachite or its metallic predecessor. Ag stability diagrams (Fig. 1D) make clear that metallic silver, silver oxides and silver sulphides are stable in most environments, but at strongly oxidizing conditions, very high pH (>12) may theoretically result in dissolution of silver species. It is unclear whether that is the case here.

4.5. Coin fissuring

It is remarkable that two of the three coins studied here (Kempraten and Krommenie) have developed intense fissuring parallel to their surface. In Kempraten, the fissures are apparent in the BE images of the corroded part of the coin, in Krommenie the whole coin seems to have transformed into a stack of thin laminae of corrosion products. As such fissuring and their orientation is not known from other types of copper alloy objects, it is likely that this is related to the manufacturing process of the coin. Inclusions may have been spread parallel to the surface during blank production, whereas the minting proper may have caused grain deformation at microscopic scales, especially if cold hammering was used. Vons (1983, 1987) theorizes that this is the cause for the laminated nature of the corroded Roman silver-copper alloy coins from Velzen and Uitgeest mentioned in the introduction. More research on uncorroded coins is needed to test whether such micro-scale orientations are indeed common in copper alloy coins, even before corrosion processes kick in.

The fissuring as seen in the Kempraten and Krommenie coins may make coins more susceptible to corrosion processes than other, more massive and more homogeneous copper alloy objects. As soon as fissures are formed, they can act as pathways for reactants into the coin, and for easy removal of dissolved corrosion products. A case in point is the presence of gypsum crystals in the core of the Krommenie coin. These must have formed after the fissures were formed, but before the metal was completely transformed into sulphides (otherwise the gypsum crystals could not have become embedded in copper sulphides). This illustrates that reactants could penetrate the coin's core already early in the corrosion process, something that is all but impossible without the fissuring.

The anisotropic pattern of transformation in the Berlicum coin is remarkable. Although no parallel fissuring has been observed, the much preferential corrosion from the rims towards the centre of the coin may also be related to the presence of defects in the metal structure due to cold hammering or other aspects of the production process.

4.6. Methodological considerations

In the present study, we used two tomographic methods to try determine the denominations of the coins. In the cases of Berlicum and Krommenie, it was done prior to destructive research, in the case of Kempraten it was done to try and glean information from an object buried in an impregnated soil block by accident. Neutron tomography proved to be well suited to obtain 3-D information. Where neutron tomography is most suited for (large) metal objects, mCT scanning proved to be effective as well in the case of small objects like coins. Both methods proved to be able to provide information that makes it possible to determine coin denominations. In future cases of such problematic corroded coins, archaeologists and numismatic specialists are advised to make 3-D tomographic recordings of such objects prior to actions that may cause irreparable damage – including splitting the concretion.

5. Conclusions

The results of this study demonstrate the complexity of copper corrosion processes in variable and changing burial conditions. Moreover, it shows how corrosion layers may help reconstruct former (changed or variable) burial conditions and past taphonomic processes.

The Berlicum coin shows that in gunmetal coins buried in gley zones *grosso mode* metallic copper and zinc are replaced by iron oxides, while the tin oxidizes but remains in place because they experience fluctuating redox conditions and ample iron species are available. The result is a coin that seems to have formed by the corrosion of an iron-tin alloy. Ongoing iron oxide precipitation result in the formation of concretions, embedding the coin remains.

The Krommenie coin shows that burial in variable coastal saline or brackish water conditions causes the formation of sulphidic corrosion products. However, the additional presence of gypsum crystals in the coins' core indicate that lamellae-like breakage patterns may result from variable redox conditions due to sulphide oxidation and reactions with calcium carbonate.

The observations on coins from freshwater (Berlicum) and coastal (Krommenie) settings show that in both settings, changing redox conditions may result in corrosion phenomena in copper alloy coins that make them – at least at first sight – easily mistaken for *subferrati*; both the laminated nature of the corroded remains (especially when in the core of the coin) and the presence of iron oxides can cause mistaken identifications, especially when no magnet is used to test the presence of remains of a metallic iron core. We cannot exclude the possibility that numismatic publications, distribution maps and databases are contaminated with such incorrect identifications of *subferrati* in the Netherlands.

The observations on the Kempraten coin demonstrate that corrosion processes can be affected as well by anthropogenic activities: Especially the alkaline environments that are formed when wood ashes become buried in an archaeological context may result in intense leaching of

copper from copper alloys, without forming much of a corrosion crust. Moreover, significant amounts of ash-derived elements like Ca can become incorporated into the corrosion layer.

Both the Kempraten and the Krommenie coin demonstrate that coins can have a tendency to fissure parallel to the surface during corrosion. This is probably due to weaknesses in their microstructure formed during coin production. This may make coins more susceptible to corrosion than other copper alloy objects.

For the future, it is advisable to make 3-D tomographic recordings prior to potentially damaging research on strongly corroded coins or other (small) metal archaeological objects.

CRediT authorship contribution statement

Conceptualization: Hans Huisman. Archaeological fieldwork and context: Tessa de Groot & Jan-Willem de Kort (Berlicum), Nils Kerkhoven & Jeroen Vaars (Krommenie), Regula Ackermann, Sarah Lo Russo & Christine Puempin (Kempraten). mCT scans: Dominique Ngan-Tillard. nCT scans: Lambert van Eijck & Zhou Zhou. Numismatic interpretation: Liesbeth Claes (Berlicum), Fleur Kemmers (Krommenie), Markus Peter (Kempraten). Micromorphology: Hans Huisman (all sites), Sarah Lo Russo & Christine Puempin (Kempraten). SEM-EDX: Ineke Joosten. Geochemical interpretation: Bertil van Os, Ineke Joosten, Hans Huisman. Writing: Hans Huisman with contributions by all.

Declaration of Competing Interest

The authors declare that they have no known competing financial interests or personal relationships that could have appeared to influence the work reported in this paper.

Data availability

All data used in this publication is included in the supplementary information.

Acknowledgements

We would like to thank Nico and Wim van Schaijk, whose kind cooperation made the research at Berlicum possible. Piet Kleij, municipal archaeologist of Zaanstad, is thanked for making the research on the Krommenie coin possible.

Mario van IJzendoorn and the late Thomas Beckman are thanked for preparing the impregnated blocks and thin sections of Berlicum and Krommenie, and of Kempraten respectively.

Paul Beliën is thanked for his help in querying the NUMIS database for *subferrati* from the Netherlands.

Andreas Pangerl helped with finding suitable reference images for the Krommenie coin in Fig. 6, and gave permission to use image 6I from www.romancoins.info

Appendix A. Supplementary material

Supplementary data to this article can be found online at https://doi.org/10.1016/j.jasrep.2022.103799.

References

Abdurakhimov, B.A., Tashmetov, M.Y., Bakirov, B.A., Yuldashev, B.S., Kichanov, S.E., Kozlenko, D.P., Ismatov, N.B., 2021. Structural Studies of the Qarakhanid Dirham Using X-Ray Diffraction and Neutron Tomography Methods. J. Surf. Invest. 15 (6), 1232–1237.

Abramson, M.G., Saprykina, I.A., Kichanov, S.E., Kozlenko, D.P., Nazarov, K.M., 2018. A study of the chemical composition of the 3rd century AD Bosporan billon staters by XRF-analysis, neutron tomography and diffraction. J. Surf. Invest. 12 (1), 114–117.

R, Ackermann, Ö, Akeret, S, Deschler-Erb, S, Häberle, S, Lo Russo, M, Peter, C, Pümpin, A, Schlumbaum, Spotlighting leftovers. The mithraeum at Kempraten (Rapperswil-Jona, Switzerland). An interdisciplinary analysis project and its initial results. in: Egri, Mariana, McCarty, Matthew (Hrsg.): *Archaeology of Mithraism. New finds and approaches to Mithras-worship*. BABESCH supplement 39. Peeters Publishers, Leuven/Paris/Bristol 2020, pp. 47-63.

Adriaens, A., Dowsett, M., Lehmann, E., Farhi, Y., Gunneweg, J., Bouchenoire, L., 2010. The coin beneath the crust: a pilot study of coins from the mediterranean coast of israel. In Holistic Qumran, Brill, pp. 11–20.

Appelo, T., Postma, D., 2004. Geochemistry, groundwater and pollution, 2nd edition,. CRC Press, p. 672 pp..

Bakirov, B., Saprykina, I., Kichanov, S., Mimokhod, R., Sudarev, N., Kozlenko, D., 2021. Phase composition and its spatial distribution in antique copper coins: neutron tomography and diffraction studies. Journal of Imaging 7 (8), 129.

T, Beckmann, Präparation bodenkundlicher Dünnschliffe für mikromorphologische Untersuchungen. *In:* K. Star (ed.) *Mikromorphologische Methoden in der Bodenkunde. Ergebnisse eines* Workshops der DBG, Kommission VII, 9. - 11. Okt. 1995 an der Universität Hohenheim. Hohenheim: Universität Hohenheim 1997 pp. , 89–103.

Bosman, A.V., 1997. Het culturele vondstmateriaal van de vroeg-Romeinse versterking Velsen 1. Universiteit of Amsterdam, p. 444 pp.. Unpublished dissertation.

Bozzini, B., Gianoncelli, A., Mele, C., Siciliano, A., Mancini, L., 2014. Electrochemical reconstruction of a heavily corroded Tarentum hemiobolus silver coin: a study based on microfocus X-ray computed microtomography. J. Archaeol. Sci. 52, 24–30.

Brookins, D.G., 1988. Eh-pH Diagrams for Geochemistry. Springer-Verlag, Berlin, p. 176.

Brousseau, L., 2010. Sybaris et les origines de la monnaies de bronze. Revue. Belge. de Numismatique. 156, 23–34.

Bude, R.O., Bigelow, E.M., 2020. Nano-CT evaluation of totally corroded coins: a demonstration study to determine if detail might still be discernible despite the lack of internal, non-corroded, metal. Archaeometry 62 (6), 1195–1201.

T, de Groot, J.W, de Kort (eds.), Veilig naar de overkant. Onderzoek naar een muntvondst uit de Romeinse tijd in het dal van de Aa bij Berlicum (gemeente Sint Michielsgestel), Rapportage Archeologische Monumentenzorg 267, Rijksdienst voor het Cultureel Erfgoed, Amersfoort 2021, 164 pp.

Doyen, J.-M., Martin, S., Peter, M., 2017. Les monnaies de bronze à « âme de fer » (nummi subferrati) dans les provinces occidentales continentales de l'Empire romain (Gaules, Germanies, Rhétie, Norique). J. Archaeol. Numismatics 7, 201–297.

M.J, Driessen, The Roman harbours of Velsen and Voorburg-Arentsburg (NL), *In*: H. Kennecke (ed.), Der Rhein als europäische Verkehrsachse – Die Römerzeit, Bonn (Bonner Beiträge zur Vor- und Frühgeschichtlichen Archäologie 16) 2014 pp. 209-228.

Gigante, G.E., Ricciardi, P., Ridülfi, S., 2005. Areas and limits of employment of portable EDXRF equipment for in situ investigations. ArchéoSciences, Revue d'Archéométrie 29, 51–59.

S.N, Herringer, K, Ryzewski, H.Z, Bilheux, J.-C, Bilheux, B.W, Sheldon, Evaluation of segregation in Roman sestertius coins. *Journal of Materials Science* 53 2018 2161–2170.

Huisman, D.J., Braadbaart, F., van Os, B.J.H., van Wijk, I., 2012. Ashes to ashes, charcoal to dust: Micromorphological evidence for ash – induced decay in early neolithic (LBK) soil features in Elsloo (The Netherlands). J. Archaeol. Sci. 39, 994–1004.

D.J, Huisman, I, Joosten, J, Nientker, Textile, In: D.J. Huisman, *Degradation of archaeological remains, SdU*, Den Haag 2009 pp. 71 - 90.

Huisman, D.J., Ishmail-Meyer, K., Sageidet, B., Joosten, I., 2017. Micromorphological indicators for degradation processes in archaeological bone from temperate European wetland sites. J. Archaeol. Sci. 85, 13–29.

Huisman, D.J., Joosten, I., 2009, Copper and copper alloys, In: D.J. Huisman, *Degradation of archaeological remains*, SdU, Den Haag 2009 pp. 111 - 124.

Ingo, G.M., de Caro, T., Riccucci, R., Khosroff, S., 2006. Uncommon corrosion phenomena of archaeological bronze alloys. Appl. Phys. A 83, 581–588.

Johnson, D.B., Hallberg, K.B., 2005. Acid mine drainage remediation options: a review. Sci. Total Environ. 338, 3–14.

Kichanov, S.E., Nazarov, K.M., Kozlenko, D.P., Saprykina, I.A., Lukin, E.V., Savenko, B. N., 2017. Analysis of the internal structure of ancient copper coins by neutron tomography. J. Surf. Invest. 11 (3), 585–589.

F, King, C, Lilja, K, Pedersen, P, Pitkänen, M, Vähänen, *An update of the state-of-the-art report on the corrosion of copper under expected conditions in a deep geologic repository*, Svensk kärnbränslehantering (SKB) 2011.

S, Lange, The Wooden Artefacts from the Early Roman Fort Velsen I, (Nederlandse Archeologische Rapporten (NAR) nr. 69), Cultural Heritage Agency of the Netherlands, Amersfoort 2021 441 pp.

J, Lendering, A, Bosman, 2012, Edge of empire. Rome's frontier and the Lower Rhine, Karwanseray BV, Zutphen, 188 pp.

B. J, Little, R.I, Ray, R, Pope, 2000b, Relationship Between Corrosion and the Biological Sulfur Cycle: A Review. *Corrosion* 56 (04) NACE-00040433.

B. J, Little, R.I, Ray, R, Pope, 2000a, The relationship between corrosion and the biological sulfur cycle. *CORROSION 2000*, OnePetro.

Little, B., Wagner, P., Mansfeld, F., 1991. Microbiologically influenced corrosion of metals and alloys. Int. Mater. Rev. 36, 253–272.

Little, B.J., Wagner, P.A., 2018. Spatial relationships between bacteria and mineral surfaces. Geomicrobiology 123–160.

Lo Russo, S., Brönnimann, D., Deschler-Erb, S., Ebnöther, C., Rentzel, P., 2022. Mithraism under the microscope: new revelations about rituals through micromorphology, histotaphonomy and zooarchaeology. Archaeol. Anthropol. Sci. 14, 46.

S, Lo Russo, Niveaulos oder abgehoben?: Geoarchäologische Untersuchungen zu Böden als Quellen zum Mithraskult in Kempraten (Rapperswil-Jona, SG). Masterarbeit 2018, Universität Basel 2021. https:// doi. org/ 10. 5281/ ZENODO. 44676 72.

M, Martinón-Torres, X, Liu, Y, Xia, A, Benzonelli, A, Bevan, S, Ma, J, Huang, L, Wang, D, Lan, J, Liu, S, Liu, Z, Zhao, K, Zhao, Th, Rehren, Surface chromium on Terracotta

Army bronze weapons is neither an ancient anti-rust treatment nor the reason for their good preservation, *Scientific Reports* 9 2019 5289.

Martinón-Torrez, M., Rojas, R.V., Cooper, J., Rehren, T.h., 2007. Metals, microanalysis and meaning: a study of metal objects excavated from the indigenous cemetery of El Chorro de Maíta. Cuba, *J. Archaeol. Sci.* 34, 194–204.

H, Matthiesen, D, Gregory, R, Sörensen, L.R, Hilbert, Long-term corrosion of iron at the waterlogged site of Nydam in Denmark: studies of environment, archaeological artefacts, and modern analogues. In: P.Dillman, G. Béranger, P. Piccardo & H. Matthiesen, Corrosion of metallic heritage artefacts. Investigation, conservation and prediction for long-term behaviour, European Federation of Corrosion Publications Number 48, Woodhead Publishing, Cambridge 2007 pp. 272-292.

McNeil, M.B., Jones, J.M., Little, B.J., 1991. Production of sulfide minerals by sulfate-reducing bacteria during microbiologically influenced corrosion of copper. Corrosion 47, 674–677.

McNeil, M.B., Little, B.J., 1999. The use of mineralogical data in interpretation of long-term microbiological corrosion processes: Sulfiding reactions. J. Am. Inst. Conserv. 38 (2), 186–199.

Miles, J., Mavrogordato, M., Sinclair, I., Hinton, D., Boardman, R., Graeme, E., 2016. The use of computed tomography for the study of archaeological coins. *J. Archaeol. Sci.: Reports* 6, 35–41.

D, Neff, E, Vega, P, Dillmann, M, Descostes, Contribution of iron archaeological artefacts to the estimation of average corrosion rates and the long-term corrosin mechanisms of low-carbon steel buried in soil. In: P. Dillmann, G. Béranger, P. Piccardo & H. Matthiesen, Corrosion of metallic heritage artefacts. Investigation, conservation and prediction for long-term behaviour, European Federation of Corrosion Publications Number 48, Woodhead Publishing Ltd. Cambridge 2007 pp. 41-76.

H. Y, Nguyen, S, Keating, G, Bevan, A, Gabov, M, Daymond, B, Schillinger, A, Murray, A., Seeing through corrosion: using micro-focus x-ray computed tomography and neutron computed tomography to digitally "clean" ancient bronze coins. *MRS Online Proceedings Library (OPL)* 2011, *1319*.

Nienhuis, J., Robbiola, L., Giuliani, R., Joosten, I., Huisman, H., van Os, B., Sietsma, J., 2016. Curly malachite on archaeological bronze: a systematic study of the shape and phenomenological approach of its formation mechanism. e-Preservation Science 13, 23–32.

J, Nienhuis, Artefact biography 2.0: the information value of corroded archaeological bronzes. Delft Technical University, Delft, PhD thesis 2017.

Orfanou, V., Rehren, T., 2014. A (not so) dangerous method: pXRF vs. EPMA-WDS analyses of copper-based artefacts. J. Anthropol. Sci. 6.

Oudbashi, O., 2018. A methodological approach to estimate soil corrosivity for archaeological copper alloy artefacts. Heritage Science 6. https://doi.org/10.1186/s40494-018-0167-4.

O, Oudbashi, R, Naseri, B, Heidarpour A, Ahmadi, A., Study on the Corrosion Mechanisms and Morphology of Archaeological Bronze Objects from a Bronze Age Graveyard in Southwestern Iran, In: C. Chemello, L. Brambilla & E. Joseph (eds.) Proceedings of the Interim Meeting of the ICOM-CC Metals Working Group September 2-6, 2019 Neuchâtel, Switzerland 2019 p. 1-8.

Ratnawulan, A.F., Hayati, S., 2017. Effect of calcination temperature on phase transformation and crystallite size of copper oxide (CuO). Powders: AIP Conference Proceedings 1868, 060009.

Rémazeilles, C., Langlet-Marzloff, V., Creus, J., Lotte, G., Deshayes, C., Baleux, F., Robbiola, L., 2020. Remarkable corrosion resumption of archaeological bronzes, induced by the oxidation of ternary Cu-Sn-S phases in atmosphere, after long-term burial with sulfides. Corros. Sci. 175, 108865.

Robbiola, L., Blengino, J.-M., Fiaud, C., 1998. Morphology and mechanisms of formation of natural patinas on archaeological Cu-Sn alloys. Corros. Sci. 40 (12), 2082–2111.

M.A, Roxburgh, S, Heeren, D.J, Huisman, B.J.H, Van Os, Non-Destructive Survey of Early Roman Copper-Alloy Brooches using Portable X-ray Fluorescence Spectrometry, *Archaeometry*, 61 1 2019 55-69.

Salvemini, F., Sheedy, K., Olsen, S.R., Avdeev, M., Davis, J., Luzin, V., 2018. A multi-technique investigation of the incuse coinage of Magna Graecia. J. Archaeol. Sci. Rep. 20, 748–755.

D.A, Scott, Copper and bronze in art. Corrosion, colorants, conservation, The Getty Conservation Institute, Los Angeles 2002 533 pp.

L, Selwyn, 2004, Metals and corrosion. A handbook for the Conservation Professional, Canadian Conservation Institute, Ottawa, 224 pp.

Stumm, W., Lee, G.F., 1961. Oxygenation of ferrous iron. Ind. Eng. Chem. 53, 143–146.

Vons, P., 1977. The identification of heavily corroded Roman coins found at Velsen: an attempt at a closer dating of the early Roman settlement "Velsen I". Berichten van de Rijksdienst voor het Oudheidkundig Bodemonderzoek 27, 139–164.

Vons, P., 1983. Metamorphosed Roman denarii from Velsen (N.H.). Helinium 23, 13–45.

Vons, P., 1987. A Second-century roman hoard of corroded denarii from uitgeest. Berichten van de Rijksdienst voor het Oudheidkundig Bodemonderzoek 37, 123–152.

Vos, P., 2015. Origin of the Dutch coastal landscape, Long-term landscape evolution of the Netherlands during the Holocene, described and visualized in national, regional and local palaeogeographical map series. Deltares, Utrecht, p. 359.

J. M, Warnett, M.A, Williams, A, Attridge, D, Mearns J.P, Vieira, Investigation of artefacts retrieved from a shipwreck of Vasco da Gama using X-ray Computed Tomography. In *2017 IEEE International Instrumentation and Measurement Technology Conference (I2MTC),* IEEE. 2017 pp. 1-6.

Wiener, M.S., Salas, B.V., Quintero-Núñez, M., Zlatev, R., 2006. Effect of H2S on corrosion in polluted waters: a review. Corros. Eng. Sci. Technol. 41, 221–227.

Zhou, Z., Plomp, J., van Eijck, L., Vontobel, P., Harti, R.P., Lehmann, E., Pappas, C., 2018. FISH: a thermal neutron imaging station at HOR Delft. J. Archaeol. Sci. Rep. 20, 369–373.